# Ano1 Antisense Therapy Improves Enamel Properties in Molars but not Amelogenesis in a Murine Model of Cystic Fibrosis

Nedjar Dinne, Vanden Bossche Arnaud, Christie Mitri, Nguyen The Nghia, Hermans Florian, Coralie Torrens, Roubier Nicolas, Elsa Vennat, Montero David, Slimani Lotfi, et al.

▶ **To cite this version:**

Nedjar Dinne, Vanden Bossche Arnaud, Christie Mitri, Nguyen The Nghia, Hermans Florian, et al.. Ano1 Antisense Therapy Improves Enamel Properties in Molars but not Amelogenesis in a Murine Model of Cystic Fibrosis. Calcified Tissue International, inPress. ⟨hal-05579219⟩

**HAL Id: hal-05579219**

**https://hal.science/hal-05579219v1**

Submitted on 3 Apr 2026

**HAL** is a multi-disciplinary open access archive for the deposit and dissemination of scientific research documents, whether they are published or not. The documents may come from teaching and research institutions in France or abroad, or from public or private research centers.

L'archive ouverte pluridisciplinaire **HAL**, est destinée au dépôt et à la diffusion de documents scientifiques de niveau recherche, publiés ou non, émanant des établissements d'enseignement et de recherche français ou étrangers, des laboratoires publics ou privés.

Copyright - All rights reserved

# *Ano1* antisense therapy improves enamel properties in molars but not amelogenesis in a murine model of cystic fibrosis

**NEDJAR Dinne[1*], VANDEN BOSSCHE Arnaud[2*], MITRI Christie[3], NGUYEN The Nghia[1], HERMANS Florian[4], TORRENS Coralie[1], ROUBIER Nicolas[5], VENNAT Elsa[5], MONTERO David[6], SLIMANI Lotfi[1,7], MAROTTE Hubert[8], CHAUSSAIN Catherine[1,9], TABARY Olivier[3], TILOTTA Françoise[1,10]**

[1]Université Paris Cité, Inserm UMR_S_1333 Oral Health, 1 rue Maurice Arnoux, 92120, Montrouge, France. [2]Université Jean Monnet, SAINBIOSE 1059, Inserm, Mines Saint-Etienne, 42000, Saint-Etienne, France. [3]Sorbonne Université, Inserm, Centre de Recherche Saint-Antoine, CRSA, 72012, Paris, France. [4]Cardiology and Organ Systems (COS), Biomedical Research Institute (BIOMED), Faculty of Medicine and Life Sciences, Hasselt University, 3590 Diepenbeek, Belgium. [5]Université Paris Saclay; Centrale-Supélec, ENS Paris-Saclay, CNRS, LMPS, 91190, Gif Sur Yvette Cedex, France. [6]Sorbonne Université, FCMat UAR2482, 75005, Paris, France. [7]Plateforme Imageries du Vivant, 1 rue Maurice Arnoux, 92120 Montrouge. France. [8]Université Jean Monnet, Department of Rheumatology, Saint-Etienne Hospital, Inserm Mines Saint-Etienne, SAINBIOSE 1059, 42000, Saint-Etienne, France. [9]AP-HP GH Nord, filière OSCAR, Paris, France. [10]AP-HP Paris Saclay, Department of Oral Medecine, Saint-Périne Hospital, 75016, Paris, France.

*Co-first

**Corresponding authors:** Françoise Tilotta françoise.tilotta@u-paris.fr and Olivier Tabary olivier.tabary@inserm.fr

## Abstract

Cystic fibrosis (CF) is a life-shortening inherited disorder caused by mutations in the gene encoding the Cystic Fibrosis Transmembrane conductance Regulator (CFTR), a protein that controls the transport of chloride ions across cell membranes. Defects in CFTR cause thick mucus, leading to chronic infections and inflammation in multiple organs.

Severe mutations, such as *G542X*, that completely abolish the function of CFTR present major therapeutic challenges. One potential approach is to stimulate an alternative chloride channel, ANO1, which is repressed in patients by the small regulatory molecule microRNA-9.

We recently showed that an antisense oligonucleotide (ASO) designed to restore ANO1 activity (*Ano1* ASO) improved respiratory and digestive functions in a CF mouse model carrying the pathogenic *G542X* variant. As patients with severe forms of CF often display enamel defects, we aimed to investigate the impact of *Ano1* ASO on enamel of *G542X* CF mice. Combining multiproxy imaging approaches, our data showed that *Ano1* ASO initiated at postnatal day 8 partially rescued the enamel properties in molars, which have mainly formed before the onset of treatment. However, it did not correct enamel maturation in the continuously growing incisor. In contrast to *CFTR*, there was no significant increase in *ANO1* expression in maturation-stage ameloblasts compared to secretion ameloblasts.

These findings suggest that while stimulating ANO1 cannot compensate for the absence of CFTR during enamel maturation, it enhances the mechanical properties of the erupted teeth, likely by improving salivary properties. This work identifies a potential avenue for mitigating dental complications in patients with severe CF mutations.

**Keywords**

Cystic fibrosis; *G542X* mutation; Antisense oligonucleotide therapy; ANO1; Enamel mineralization; Ameloblast function

## Introduction

Cystic fibrosis (CF) is a common autosomal recessive genetic disorder, particularly prevalent among individuals of Caucasian descent, with an estimated 2,500 to 4,000 new cases diagnosed annually [1]. CF pathology is caused by mutations in the *CFTR* (*Cystic Fibrosis Transmembrane conductance Regulator*) gene, which encodes a chloride channel essential for maintaining the proper viscosity and hydration of mucus at the surface of the epithelial cells [2]. Although respiratory complications are the most life-threatening, CF can also affect other organs, including the gastrointestinal tract, pancreas, liver, and reproductive system [3]. In the respiratory tract, CF leads to the production of thick mucus, chronic bacterial infections, inflammation, and progressive tissue damage. These chronic infections are caused by various bacterial species that thrive in the viscous mucus and contribute to tissue destruction [4–6]. The most common CF-causing mutation is the *F508del* variant, while the *G542X* variant introduces a premature codon stop, resulting in a truncated CFTR protein. Both mutations are associated with a severe disease phenotypes due to the absence of functional CFTR on the cell surface [7-9].

CF patients frequently present with developmental defects of enamel, including enamel hypoplasia and/or hypomineralization [10-11]. These constitutive enamel defects increase the vulnerability to oral conditions such as dental caries, erosion, and hypersensitivity, which can negatively impact patients' quality of life by causing pain, early tooth loss, and impaired masticatory function [12]. Enamel defects have also been reported in rodent and porcine models of CF, making them valuable tools for studying the pathophysiology of amelogenesis and evaluating the effects of new treatments on enamel [13-17]. Amelogenesis occurs in two major stages, secretion and maturation, which initiate and orient the nanostructure of hydroxyapatite to form the prisms and depend on precise pH regulation [18]. Enamel defects associated with CF are thought to result from dysfunction of CFTR, which is expressed at the apical end of maturation-stage ameloblasts (mAB) [19]. CFTR contributes to the ion balance during enamel maturation, particularly in the secretion of bicarbonate, which is crucial for neutralizing acid and maintaining pH homeostasis. Although pH regulation is vital for proper enamel mineralization, the precise mechanisms by which *CFTR* mutations lead to enamel hypomineralization remain poorly understood [20-21]. It is hypothesized that impaired ion transport by CFTR and by extension, associated ion channels disrupt ameloblast function and enamel mineralization. Additional contributing factors may include CF-related malabsorption,

nutritional deficiencies, and long-term antibiotic use, all of which may exacerbate enamel defects in CF patients [22].

Despite significant advances in CF treatment, particularly the development of CFTR modulators designed to restore the function of defective CFTR, these therapies are not effective for all patients [23-24]. Notably, approximately 15% of individuals with CF, including those carrying class I mutations such as *G542X*, do not benefit from these modulators. *CFTR* mutations are categorized into six functional classes according to their impact on the CFTR protein. Class I mutations result in a complete absence of protein due to nonsense or frameshift mutations that lead to premature stop codons. Because no functional protein is produced, modulators that improve CFTR folding or gating (used in other mutation classes) are ineffective in these patients [25]. This limitation has prompted the investigation of alternative therapeutic strategies, including approaches that target other ion channels. One promising target is ANO1 (also known as TMEM16A), a calcium-activated chloride channel that is functionally comparable to CFTR in function, including its role in bicarbonate secretion and chloride ion transport [26-28]. Similar to CFTR, ANO1 is expressed in epithelial cells and contributes to ion homeostasis, hydration, cell proliferation, and migration [29-31].

In CF patients, *ANO1* expression is downregulated in bronchial epithelial cells [32], partly due to the binding of microRNA-9 (miR-9) to the 3′ untranslated region (3′UTR) of *ANO1* mRNA, which blocks its translation [25, 33-34]. A novel antisense oligonucleotide therapy (*Ano1* ASO) has been developed to target the *Ano1* 3′UTR region, preventing miR-9 binding and thereby relieving translational repression of ANO1 [25]. Previous studies in CF mouse models have shown that *Ano1* ASO treatment enhances mucus clearance, reduces airway obstruction, and improves survival [35], suggesting its potential as an alternative therapy for CF patients, including those unresponsive to CFTR modulators. Furthermore, we recently reported that *Ano1* ASO treatment improved life expectancy of CF mice (*F508del* and *G542X*), by activating chloride efflux without any toxicity observed even after one year of treatment [36]. However, the potential effect of this new therapy on enamel defects remains unknown. The present study aimed to investigate the impact of *Ano1* ASO treatment on enamel formation, morphology, mineral content, and biomechanical properties in the *G542X* CF murine model [32]. In this study, we investigated the enamel of the molars, which had mostly formed before treatment, and of the continuously growing incisors, which formed under *Ano1* ASO treatment, using multiproxy imaging analyses. This study included tissue clearing and confocal reflexion microscopy (TC-CReM) to observe hydroxyapatite crystal structures *in situ*. Our data show that

*Ano1* ASO treatment leads to modest improvement in enamel mineralization and biomechanical properties in the first molar but does not correct amelogenesis in the continuously growing incisor.

## Materials and Methods

### Animal distribution, biological and technical replicates

All experimental procedures were approved and conducted in accordance with the guidelines of our Institutional Animal Care and Use Committee (protocol numbers 38427-2022091211033928 v8 and 43883-2023062011193610 v7, Ethical Committee for Laboratory Animal Care Charles Darwin France). A total of 32 mice were included in this study: 16 aged 2–3 months and 16 aged 4–6 months. We used mice with the pathogenic variants *G542X*, derived from the 129-*Cftr*$^{tm1Eur}$ strain [25]. At each age, animals were assigned to four experimental groups (n = 4 biological replicates per group): (1) WT, (2) *G542X*, (3) *G542X* Control ASO, and (4) *G542X Ano1* ASO. *G542X* mice were treated (20 µl per injection, at the final concentration of 10 mg/kg) with *Ano1* ASO or control ASO via subcutaneous injection on days 8 and 11, and subsequently every 15 days post-weaning until euthanasia. Two time points were selected to assess the time-dependent effects of treatment. Wild-type and untreated *G542X* mice were euthanized at the same time points to serve as controls. The sequence of *Ano1* ASO used is: AATCTTTGGTAGTAA, and the control ASO sequence is: ACGTCTATACGCCA.
Both sexes were included. For each experimental group (n = 4), the cohort consisted of three males and one female. For analyses conducted with n = 3 biological replicates (nanoindentation, SEM, and TC-CReM), groups included two males and one female. The same sex distribution was applied to the additional WT mice used for histology and RT-qPCR. Sex was not analyzed as an independent biological variable in the present study. A summary of animal allocation, including age, experimental group, number of biological replicates, sex distribution, and analyses performed, is presented in Table 1.

| Analysis | Age (months) | Groups | n biological replicates | Sex (M/F) | Notes |
|---|---|---|---|---|---|
| Photographs | 2–3 & 4–6 | WT, *G542X*, Control ASO, *Ano1* ASO | 4/group | 3/1 | — |
| Micro-CT | 2–3 & 4–6 | WT, *G542X*, Control ASO, *Ano1* ASO | 4/group | 3/1 | — |
| Nanoindentation | 2–3 | WT, *G542X*, Control ASO, *Ano1* ASO | 3/group | 2/1 | One excluded per group; same mice used for SEM + TC-CReM |
| SEM | 2–3 | WT, *G542X*, Control ASO, *Ano1* ASO | 3/group | 2/1 | Same mice |
| TC-CReM | 2–3 | WT, *G542X*, Control ASO, *Ano1* ASO | 3/group | 2/1 | Same mice |
| ANO1 expression by immunohistochemistry | 3 | WT | 3 | 2/1 | Additional animals |
| *Ano1* expression by RT-qPCR | 3 | WT | 3 pooled | 2/1 | RNA pooled; qPCR in triplicate |

**Table 1**: Animal allocation including age, experimental group, number of biological replicates, sex distribution, and analyses performed

**Sample Preparation**

Following euthanasia by carbon dioxide inhalation, the heads were collected and fixed in a large volume of 4% paraformaldehyde (PFA) for 72 hours at 4°C. Samples were then rinsed five times in 1x phosphate-buffered saline (PBS) for 10 minutes each. After rinsing, the perioral skin was carefully incised to expose the incisors. The heads were positioned in an upright orientation and stabilized using forceps to allow for standardized anterior visualization of the incisors. Photographs were captured using a Nikon D5600 DSLR camera.

**Micro-CT Acquisition and Image Analysis**

Micro-computed tomography (micro-CT) imaging was performed using a Quantum FX µCT scanner (Caliper, PerkinElmer®) at the PIV micro-CT facility (Université Paris Cité, Inserm

UMR_S 1333 Oral Health). Mouse heads were positioned vertically on the scanning bed to ensure full capture of the mandibles. The 3D scans were performed with acquisition parameters described as follows: voxel resolution of 20 µm, field of view (FOV) of 10 mm, acquisition time of 3 minutes, X-ray tube current of 160 µA, voltage of 90 kV and aluminum filter (100 µm). Image analysis was carried out using Analyze 14.0® (AnalyzeDirect) and OsiriX® (Pixmeo) software. For all analysis, only the left hemimandibles were examined to ensure consistency across samples. Three-dimensional reconstructions of the enamel were generated in OsiriX, applying a minimum segmentation threshold of 4500 Hounsfield Units (HU) to distinguish enamel from dentine and alveolar bone. Cropping was performed to retain only the left hemimandible and remove surrounding anatomical structures. Quantitative analyses were conducted using Analyze 14.0, which calculated the enamel surface area, volume, and density based on the same segmentation threshold used in OsiriX®. A set of phantoms calibrated in mg of hydroxyapatite per $cm^3$ was used to convert CT intensity in Hounsfield unit. To facilitate segmentation, 3D images were reoriented to align the mouse mandible horizontally. Following reorientation, enamel segmentation was applied to both the mandibular first molar and incisor for detailed phenotypic characterization. A final cropping step was used to eliminate background artifacts and isolate the left first molar and incisor for analysis.

**Nanoindentation**

Each hemi-mandible was sectioned mesial to the first molar (M1) using a diamond disc saw (Accutom-5®, Struers). Slices 2 mm thick were obtained, encompassing M1 and the anterior portion of the second molar (M2). Each section was affixed to a glass slide using cyanoacrylate adhesive and embedded in methyl methacrylate dental resin using a plastic mold. Following resin polymerization, samples were re-sectioned to maintain alignment with the initial cutting plane. Manual polishing was carried out in successive stages: initial polishing with P600 grit sandpaper (Aluminium oxide) down to the beginning of M1's mesial root, followed by P1200 grit to reach the region of interest at the mesial root of M1, corresponding to the onset of enamel mineralization in mouse incisor. Final polishing was performed with P2400 grit to expose the mid-root region of M1, revealing the complete pulp chamber. Throughout the polishing process, samples were examined under an optical microscope (InfiniteFocus G5plus® – Bruker Alicona) to ensure proper surface preparation and anatomical orientation. After polishing, samples were ultrasonically cleaned for 45 seconds to eliminate any remaining abrasive or resin particles. A final surface finish was achieved using a felt disk and 3µm diamond suspension to remove micro-scratches and produce a smooth, reflective surface suitable for nanoindentation.

Optical microscopy was first used to image the enamel of M1 and the incisor, allowing for precise mapping of future indentation sites using ImageJ® software. Nanoindentation tests were performed using an NHT3 nanoindenter (Anton Paar, USA) equipped with a Berkovich indenter tip. Area function calibration was performed with fused silica using its known homogeneous Young's modulus prior to the tests. The space between the indents was a minimum of 40 µm and the indentations were performed in the middle of the enamel thickness.

Based on the mapped regions, 10 to 15 indentations were applied per sample, each with a maximum penetration depth of 3 µm. This depth was selected to obtain an average enamel value by encompassing several prisms, thereby averaging local tissue heterogeneities while minimizing potential artefacts related to surface heterogeneity between the different groups of mice studied.

The indentation parameters were as follows: maximum depth of 3000 nm, loading rate of 6000 nm/min, unloading rate of 6000 nm/min, a pause of 2 seconds at maximum load, an approach distance of 5000 nm, and an approach speed of 8000 nm/min. Mechanical properties, including hardness and elastic modulus, were calculated using the Oliver and Pharr method, based on the unloading portion of the force-displacement curve [37].

**Scanning electron microscope (SEM) Analysis**

Following nanoindentation, the samples were re-polished using P2400 grit sandpaper to remove residual indentations. To clean the surface, samples were treated with 5% sodium hypochlorite for 2 minutes, followed by three rinses with distilled water (1 minute each). To prepare the samples for SEM, the methyl methacrylate resin was dissolved using acetone to prevent charging up around the biological tissue and possible outgassing. To expose the underlying enamel prism structure, the enamel surface was etched with 37% phosphoric acid for 1 second (due to the highly demineralized enamel in CF mice), then rinsed thoroughly (3x3 minutes with distilled water). Samples were subsequently dried using liquid carbon dioxide to avoid deformation or cracking. They were mounted on aluminum stubs using conductive silver adhesive and sputter-coated with a thin layer of gold (40 nm) to ensure adequate electronic surface conductivity. SEM imaging was performed using a Hitachi SU-70 Schottky gun field emission scanning electron microscope (FESEM). Multiple micrographs were acquired from the incisors and molars at magnifications ranging from x30 to x5,000 to assess microstructural features.

**Tissue Clearing and Confocal Reflection Microscopy (TC-CReM)**

One hemimandible per experimental group was fixed in 4% PFA, rinsed in 1x PBS, and stained with rhodamine 6G (0.3% in absolute ethanol) under vacuum for 2 hours. The specimens were then stored at 4°C for at least 24 hours in the staining solution (rhodamine 6G).

After staining, the hemimandibles were rinsed several times in absolute ethanol for 30 minutes under vacuum to remove excess dye and microbubbles. They were sectioned without drying using a diamond wire saw (WELL W3500) in absolute ethanol. Two or three sagittal sections were obtained per specimen, each 0.4 mm thick. Section debris was gently removed by immersing the sections in 1.5 ml tubes containing absolute ethanol for up to 5 minutes. Sections were kept stained, while excess dye remained in the supernatant. Ethanol was carefully removed without drying the samples. For tissue clarification, non-demineralized sections were immersed in a clarifying solution based on the modified Murray method, consisting of benzyl alcohol and benzyl benzoate (1:9, v/v), adjusted to a refractive index of 1.565 [38]. Samples were kept in the clarifying solvent for at least 24 hours before observation. Confocal imaging was performed with a Zeiss LMS 800 confocal microscope and ZEN blue software using oil immersion objectives (Zeiss Plan-Apochromat® 40x/1.3 oil and 63x/1.4 oil). Rhodamine 6G was excited at 565 nm and reflection with emission/detection at 640 nm. Acquisition and post-processing parameters were strictly identical for all samples. The principle of the TC-CReM technique used here is described in detail in Supplementary Material 1.

**Single-cell transcriptomics**

Evaluation of *Cftr* and *Ano1* gene expression in mouse enamel organ was conducted using previously established and publicly available single-cell transcriptomic atlases of mouse tooth (in-house; and available at doi.org/10.17632/2kskdknngb.1, dataset V1, published 3 Oct 2022) [39]. This resource combines 9 publicly available single cell transcriptomic datasets of postnatal mouse molars and incisors, spanning early postnatal to adult life. Gene expression analysis was performed on the subset of all dental epithelial populations, as indicated in Fig. 6A, which includes the entire ameloblast lineage (from pre-ameloblast to secretory- and maturation stage ameloblasts). Feature plots were generated using the FeaturePlot function of the Seurat package (v4.0.1) using SoupX-corrected (to control for ambient/background RNA) and normalized counts [40-41]. All analysis code used to develop the atlas is available on GitHub (https://github.com/fhermans27/scRNAseq-tooth-atlas).

**Reverse Transcription Quantitative PCR (RT-qPCR)**

Incisors from 2-3-month-old WT mice were meticulously dissected from the alveolar bone. As outlined by Houari et al. (2018), the secretion and maturation stages of the enamel organ were collected separately [42]. In addition, the salivary gland was harvested as a positive control. The tissues were then lysed immediately using buffer RLT (RNeasy Micro Kit, Qiagen, Venlo, Netherlands). The lysate was stored at -80°C, pending subsequent processing.

The RNA extractions were performed using the RNeasy Micro Kit (Qiagen, Venlo, Netherlands). The reverse transcription process was conducted using random primers, employing the Verso cDNA Synthesis Kit (Thermo Fisher Scientific, Waltham, MA).

Quantitative PCR (qPCR) was performed using the StepOnePlus™ Real-Time PCR Systems (Applied Biosystems, Thermo Fisher Scientific) with TaqMan™ gene expression assays. Relative quantification of RNA levels was carried out using the $2^{-DDCT}$ method and normalized to the expression levels of *Gapdh* (Table 2). Each sample was assessed in duplicate.

| | RefSeq | Reference | Amplicon size | Provider |
|---|---|---|---|---|
| *Gapdh* | NM_001289726.1 | Mm99999915_g1 | 109 | Thermo Fischer Scientific |
| *Ano1* | NM_001242349.1 | Mm00724407_m1 | 63 | Thermo Fischer Scientific |
| *Cftr* | NM_021050.2 | Mm00445197_m1 | 88 | Thermo Fischer Scientific |

**Table 2** : Details of TaqMan probes used for RT-qPCR analysis. The target genes (Gapdh, Ano1, and Cftr) are listed with their corresponding RefSeq accession numbers, commercial assay references and amplicon sizes

**Immunohistochemistry**

Hemimandible sections were dehydrated using an ascending ethanol concentration series. Endogenous peroxidases were blocked in 0.4% hydrogen peroxide in methanol. After extended rinsing in PBS, background activity was blocked at room temperature for 90 minutes in 1% bovine serum albumin (BSA) in PBS. Rabbit polyclonal ANO1 antibody (Proteintech, 12652-1-AP) were used at 1/300 dilution. Sections were treated overnight in a moist chamber at 4°C and further incubated for 60 minutes with a polyclonal swine anti-rabbit immunoglobulin-G peroxidase conjugate (Dako, Denmark). Peroxidase labeling was revealed using 3-3-diaminobenzidine tetrahydrochloride (DAB, Sigma-Aldrich) diluted in 5 mL of $H_2O$. To

exclude nonspecific binding, controls were carried out by omitting the primary antibody. Lung sections sampled in 3-month-old WT mice and similarly processed were used as positive control (Supplementary Material 2).

### Statistical Analysis

All statistical analyses were conducted using GraphPad Prism 9 (GraphPad Software, San Diego, CA, USA). Animals were randomly allocated to experimental groups, and all data processing was performed blindly to minimize bias. Data are presented as mean ± standard deviation (SD). Differences among three groups or more were assessed using one-way analysis of variance (ANOVA) or two-way ANOVA, followed by Tukey's Honestly Significant Difference (HSD) test as a post hoc analysis to identify specific group differences where applicable. Statistical significance was defined as $p < 0.05$. Pearson's correlation coefficients were calculated to evaluate linear relationships between variables. In all figures, statistical significance is denoted as follows: NS: No Significant, *$p < 0.05$, **$p < 0.01$, ***$p < 0.001$, and ****$p < 0.0001$.

## Results

### *Ano1* ASO treatment fails to restore enamel mineralization in the continuously growing incisor but improves the first molar

Visual examination of the enamel at both 2-3 months and 4-6 months revealed striking differences in the appearance of the incisors between *G542X* CF mice (either untreated, control ASO-treated or *Ano1* ASO-treated) and WT mice (Fig.1). CF mice consistently exhibited severe enamel hypomineralization, manifesting by brittle teeth that were prone to cracking and markedly white in color, indicative of enamel disorganization. In contrast, WT mice displayed well-mineralized enamel enriched with iron, conferring a characteristic yellowish hue [43]. However, the enamel surface of *Ano1* ASO-treated *G542X* mandibular incisors appeared slightly smoother and less abraded, compared to control ASO-treated mice.

We next performed micro-CT analysis to determine the enamel surface area, volume, and density of the continuously growing mandibular incisor at both time points (Fig. 2). Sagittal reconstructions revealed delayed mineralization in CF incisors, regardless of the treatment, with a pronounced decrease in enamel volume and density, as well as porous enamel structure

(Fig. 1B). Enamel mineralization was observed to begin under the second (M2) and third (M3) molars in the WT incisors. In contrast, in the CF incisors, it was at best visible under the first molar (M1) or beyond, regardless of the group. Consistently, measurement of the incisor enamel surface under the first (M1) and the second (M2) molars showed that enamel thickness was significantly lower in all CF mice compared to WT ($p < 0.0001$) (Fig. 2A-B). Furthermore, enamel volume and density were both significantly lower in the incisors of the CF groups than in the WT group ($p < 0.0001$) (Fig. 2C-D).

Analysis of the first lower molar (M1) of untreated *G542X*, and control ASO *G542X* CF mice also showed significantly lower enamel volume and density compared to WT at both time points, albeit more significant at the longer time point (Fig. 3A-B). In contrast, *Ano1* ASO-treated mice showed improved enamel volume and density in molars. At the 2–3 month time point, these values were not significantly different from those of the WT group ($p > 0.05$).

These data show that enamel volume and mineral density of both the mandibular incisor and the first molar in *G542X* CF mice are markedly reduced. Compared to untreated or control-treated mice, Ano1 ASO treatment shows a slight beneficial effect on enamel mineralization in molars but does not restore enamel mineralization in the incisor.

### *Ano1* ASO treatment fails to restore enamel biomechanical properties in the continuously growing incisor, but improves the first molar

Next, nanoindentation assays were performed to assess the biomechanical properties of the enamel in the incisor and first molar of WT, *G542X*, control ASO-treated *G542X*, *Ano1* ASO-treated *G542X* 2-3-month-old mice. For the incisor, all the CF mice, whether treated or untreated, exhibited significantly lower enamel hardness and elastic modulus compared to WT mice, indicating decreased enamel resistance to deformation (Fig. 3C).

In contrast, in the first molar, the enamel from *Ano1* ASO-treated mice exhibited significantly higher hardness than enamel from control ASO-treated mice ($p < 0.01$), which is consistent with the micro-CT findings (Fig. 3D). Furthermore, there was no significant difference in enamel elasticity between WT and treated or not treated CF mice, suggesting relative resistance of molar enamel to biomechanical degradation.

### The surface of molars is less altered in *Ano1* ASO-treated mice

We then examined the enamel structure of the incisor and first molar in CF and WT mice using scanning electron microscopy (SEM) on frontal sections of the mandible prepared at the level of the mesial aspect of M1 (Fig. 4). For both molar and incisor, WT mice displayed well-

organized prismatic enamel, characterized by a robust interweaving of the prisms. In contrast, *G542X* mice exhibited an accumulation of non-mineralized matrix in the incisor, with prisms that were difficult to distinguish, indicating delayed maturation. As observed with micro-CT and mechanical findings, no differences were observed between *Ano1* ASO- and control ASO-treated CF mice (Fig. 4A). In the molar, the prismatic structure was still present in all the CF groups, although less defined than in WT, with patches of non-mineralized matrix within the bulk of the enamel. In addition, the surface was eroded with cracks and fractures of the outer enamel layer in both untreated and control ASO-treated CF mice. Such fractures were visible at a lesser degree on the surface of the *Ano1* ASO-treated group (Fig. 4B).

**Altered ameloblast morphology and absence of mineralized enamel in CF mice revealed by TC-CReM**

To further assess amelogenesis in CF mice, we used an innovative histological imaging method, TC-CReM, applied here to non-demineralized mandibles. This straightforward method, merging histological and optical techniques, allows for the simultaneous collection of fluorescence and reflection signals. It enables the observation of cellular structures, extracellular matrices, and mineralization interfaces in fluorescence, as well as the reflection of secretion and maturation dynamics of hydroxyapatite crystals during enamel formation. The TC-CReM method implemented here optimizes the epifluorescence and optical reflection capabilities of laser scanning confocal microscopy (LSCM) to achieve imaging at its maximum depth. (Fig. 5 and Supplementary Video).

At the level of the incisor, TC-CReM revealed the presence of hypomineralized enamel matrix in *G542X* mice treated with either control ASO or *Ano1* ASO, particularly in the region located beneath M1, regardless of ASO treatment. In addition, the morphology of the dental epithelium appeared altered in CF mice whatever the treatment was. The mAB and papillary layers in these CF mice were disorganized and flattened, in contrast to the well-organized dental epithelium observed in WT mice (Fig. 5A and Supplementary Video Incisor).

In molars, TC-CReM revealed enamel hypomaturation in CF mice, regardless of ASO treatment, whereas in WT, a well-organized mineralized prismatic organization was observed (Fig. 5B and Supplementary Video Molar).

These results indicate that *Ano1* ASO treatment does not restore amelogenesis in *G542X* CF mice. Furthermore, the disrupted morphology of the dental epithelium during the maturation stage probably causes mineral deposition to fail, suggesting that CFTR deficiency has a dual impact on ion transport and ameloblast integrity during amelogenesis.

**Differential expression of CFTR and ANO1 in secretory and maturation ameloblasts**

We next studied the expression of ANO1 in ameloblasts. We first analyzed single-cell RNA-sequencing data from a publicly available mouse tooth atlas [39]. The expression profile showed that in mAB, *Cftr* was expressed at higher levels than *Ano1* (Fig. 6A). We next performed RT-qPCR analyses on micro-dissected sAB and mAB obtained from the continuously growing incisors. The results showed that *Cftr* expression was significantly up-regulated in mAB compared to sAB ($p < 0.05$), which was not the case for *Ano1* expression ($p > 0.05$) (Fig. 6B). *Ano1* expression in mAB was confirmed at the protein level by immunohistochemistry (Fig. 6C). These results suggest that CFTR may play a more prominent role than ANO1 in ameloblasts, particularly at the maturation stage when ion transport is crucial for proper enamel mineralization.

## Discussion

In class I CF mutations, like the *G542X* nonsense mutation, the absence of CFTR protein renders treatments with modulators that improve CFTR folding or gating (effective for other mutation classes) ineffective. In the present study, we investigated the effect of *Ano1* ASO (an antisense oligonucleotide targeting *Ano1* mRNA) on enamel defects in a *G542X* mutation-harboring murine model, a new treatment developed for Class I CF mutations. We performed a multiscale analysis of the enamel, ranging from macroscopic morphology to microstructural characterization, including a novel method that combines tissue clearing and confocal reflection microscopy. Our data showed that *Ano1* ASO treatment improved the mechanical properties of molar enamel but did not correct enamel mineralization in the continuously growing incisor.

Altered enamel mineralization has been repeatedly described in small and large animal models of CF, including *Cftr* knock out (KO) rat, mouse and porcine models [13-17, 44], as well as in knock in (KI) rat and porcine models bearing the *F508del* variant [15, 17, 45], which is the most prevalent variant in humans [3]. Here, our data revealed that the *G542X* CF mouse model also exhibited a severe enamel phenotype, with alterations in both molars, which have formed during the early days of the animal's life, and in the continuously growing incisor. Overall, these studies showed that CF animal models effectively mimicked the enamel defects observed in CF patients, making them useful for evaluating how CF treatments affected enamel mineralization, particularly in the continuously growing incisor model [46].

Macroscopic examination of the incisors showed enamel hypomineralization in *G542X* mice, with teeth appearing brittle and noticeably white. Under normal conditions, murine enamel displayed a yellow color due to iron infusion, which contributed to improved mechanical properties and enhanced resistance against acid attacks [43]. In contrast, enamel discoloration, as seen here in *G542X* mice, was a marker of *amelogenesis imperfecta* in rodents [47-48]. Our findings were consistent with the macroscopic observations previously made in a *G542X* rat model, which also displayed enamel discoloration in the incisors [9].

Although *Ano1* ASO–treated mice showed a slightly improved morphology of the erupted part of the incisors, with smoother and less abraded enamel surfaces compared to control ASO-treated mice, micro-CT imaging did not reveal any significant improvement. Enamel volume and density remained significantly lower in the incisors of all the *G542X* CF mice compared to WT mice, and there was a major delay in mineralization onset, as previously reported by our team in the *F508del* rat model [17]. These findings were further supported by the nanoindentation analysis, which showed no improvement in the mechanical properties of the incisors of *Ano1* ASO-treated mice compared to untreated CF mice or those treated with ASO controls. Furthermore, in CF mice, regardless of the condition, SEM revealed non-mineralized enamel matrix on frontal sections made at the level of M1, whereas in WT mice, the incisor's maturation process was well advanced at this level. Taken together, these data demonstrated that *Ano1* ASO treatment had no measurable effect on enamel mineralization and that the continuously growing incisor is not an ideal model to evaluate its positive outcome.

In contrast, the molars, which form during the early days after birth to be functional at weaning, showed increased enamel volume and mineral density in *Ano1* ASO–treated mice compared to untreated *G542X* CF mice, indicating a partial therapeutic effect of the treatment. In addition, SEM revealed less damage to the enamel surface, and nanoindentation revealed an improvement in enamel hardness. These data raise two hypotheses. Either the role of ANO1 differs during enamel maturation between molars and incisors, or the treatment indirectly impacts enamel surface integrity after tooth eruption by improving the quality of the saliva. Supporting this latter hypothesis, it has been demonstrated that ANO1 is highly expressed in the salivary glands, where it facilitates bicarbonate secretion and, consequently, salivary buffering [49-50]. Furthermore, because *Ano1* ASO treatment was given at post-natal day 8, when amelogenesis in molars is almost complete [51], especially in the first molar that was the focus of our investigations, the benefits are likely to be indirect and attributed to improved saliva properties.

We proposed that the enhanced salivary bicarbonate content associated with *Ano1* ASO treatment could improve saliva properties, raising the oral pH, resulting in decreased enamel erosion and preserved molar enamel integrity, as previously demonstrated for the CFTR channel [52]**.** Both SEM and TC-CReM, a new method allowing observation of the mineralized matrix and of the dental epithelium at the same time on undecalcified samples, revealed marked structural disruption of the enamel prisms in CF molars with accumulation of hypomatured enamel matrix, which was not improved by *Ano1* ASO treatment.

It has been reported that patients with CF have a higher prevalence of enamel developmental defects than individuals without CF [12]. Consequently, patients with CF are more susceptible to dental pathologies such as caries and premature tooth wear. Furthermore, salivary dysfunction has also been reported in CF patients [53], further increasing their susceptibility to these pathologies. CFTR is known to play a critical role in bicarbonate ion secretion, which regulates salivary pH homeostasis [54]. Furthermore, CFTR is highly expressed in salivary glands in both mice and humans [55-56]. A dysregulated oral pH, resulting from CFTR dysfunction, could promote gradual enamel erosion, particularly in molars, where enamel is not continuously renewed, unlike in incisors. Interestingly, the mouse model of CF also exhibits abnormal saliva with decreased bicarbonate secretion, resulting in a significant drop in pH [45]. Here, we showed that the erupted enamel of untreated and control ASO-treated mice was more severely damaged than the erupted enamel of treated mice. Taken together, these findings indicated that improved enamel properties observed mainly in molars and, to a lesser degree, on the erupted part of the incisors may be an indirect consequence of the treatment on the saliva. This urges the need to assess the benefit of *Ano1* ASO treatment on salivary glands in future studies. Nevertheless, saliva correction aligns with our recent findings, where we demonstrated that this strategy could increase ANO1 chloride channel expression and activity in various tissues [36]. It may be hypothesized that early *Ano1* ASO treatment in CF patients with a Class I mutation could help preserve erupted enamel by enhancing saliva production. Indeed, murine molars are a model more similar to human teeth than the continuously growing incisor.

The limited effectiveness of *Ano1* ASO on amelogenesis may be attributed to a minor role of ANO1 in enamel maturation by ameloblasts compared with CFTR. Strengthening this hypothesis, the tooth atlas and qPCR analysis on micro-dissected ameloblasts showed that the expression of *Cftr* was increased in maturation ameloblasts compared with secretory ameloblasts. Future studies are needed to confirm the minor role of ANO1 in enamel

maturation. Interestingly, other bicarbonate transporters such SLC26A1, SLC26A6, and SLC26A7 have been shown to interact with CFTR in mouse maturation ameloblasts, contributing to enamel matrix pH regulation [57]. Similarly to CFTR, these anion exchangers were also upregulated at the maturation stage, but their individual deletion was not linked to significant enamel changes, suggesting that they compensate each other. However, they are not sufficient to make up for CFTR deficiency. Beyond enamel, *Ano1* ASO systemic treatment may have consequences on other skeletal tissues that remain to be evaluated. While enamel-forming cells (ameloblasts) are not osteocytes, these findings highlight how membrane channel function and cell integrity broadly affect mineralizing cells [58]. In this regard, Tuladhar et al. recently provided a comprehensive overview of approaches for evaluating bone and cartilage toxicity in drug development, which may be useful for future studies evaluating the potential toxicity *Ano1* ASO on bone cells [59].

CF is often associated with kidney abnormalities, which affect systemic mineral homeostasis [60-62] resulting in bone loss [63]. Given that amelogenesis is also a biomineralization process dependent on the mineral homeostasis [64], it can be hypothesized that it might also be affected by the kidney disturbance associated with CF, although further studies are needed to confirm this. Previous studies have shown that mutations in claudin genes (e.g., *CLDN16*, *CLDN19*) encoding tight junction proteins expressed both in the kidney and in ameloblasts lead to amelogenesis imperfecta in humans and in enamel hypomineralization in mouse models, with defects resembling those observed in CF mice, albeit less severe [65-67].

Finally, this study highlights the potential of photonic imaging using TC-CReM, which combines fluorescence and reflection in optically clarified tissues, for investigating enamel, the most challenging mineralized tissue.

One of the key advantages of TC-CReM was that it did not require prior demineralization, thereby preserving the native structure of dental tissues. This was particularly critical for studying enamel, where standard demineralization-based approaches often result in the loss of essential mineralization information. By preserving mineral content, TC-CReM facilitated the direct observation of immature enamel, an area that was difficult to distinguish using micro-CT because its low mineral density closely resembled that of adjacent alveolar bone. As a result, TC-CReM provided complementary data to micro-CT, revealing regions of early enamel mineralization that would otherwise remain undetected.

This technique detected immature enamel through local changes in the refractive index of the tissue, which generate reflected light and make these structures visible under confocal reflection imaging. This optical property allowed TC-CReM to distinguish enamel at various stages of mineralization along the entire length of the incisor, offering a dynamic and continuous view of enamel development. With its ability to preserve tissue integrity and reveal fine structural details, TC-CReM represents a valuable tool for advancing our understanding of mineral homeostasis in situ, particularly in difficult-to-study tissues such as dentin, bone, and especially enamel [68].

## Conclusion

This study demonstrated that *Ano1* ASO treatment did not rescue enamel mineralization or correct amelogenesis in CFTR-*G542X* mice, likely due to the limited role of ANO1 in maturation-stage ameloblasts. However, the therapy partially improved the biomechanical properties of erupted molar enamel, suggesting an indirect effect possibly mediated through enhanced salivary gland function. These findings underscored the importance of CFTR in enamel maturation and support further investigation into *ANO1*-targeted therapies not only for respiratory outcomes, but also for oral health preservation in CF patients with Class I mutations.

## Figure legends

**Fig. 1** (a) Representative pictures of incisors from WT mice, *G542X*, *G542X*, *Ano1* ASO-treated, or control ASO, aged 2 to 3 months and 4 to 6 months. Incisors from transgenic, *G542X* Control and *G542X Ano1* ASO mice show brittleness, cracks, and white staining with areas of hypo mineralized enamel represented by white arrows. (b) 3D representation of the hemi-mandibles highlighting the volume and density of incisor and molar enamel using OsiriX segmentation software (n = 4 mice per group). Scale bars: 1 mm.

**Fig. 2** Micro-CT imaging and quantitative analysis of the incisor from WT mice, *G542X*, *G542X* Control ASO and *G542X Ano1* ASO, aged 2 to 3 months and 4 to 6 months. (a) 2D scan of frontal sections of incisors at the level of the different roots of the first (M1) and second (M2) molars using the OsiriX software. Scale bars: 1 mm. (b) Quantification of enamel surface in the incisor at the level of the first molar (M1M: mesial root M1 and M1D: distal root M1) and second molar (M2M: mesial root M2 and M2D: distal root M2), performed using Analyze 14.0

software. Statistical tests using Two-Way ANOVA were performed for this analysis ****$p <$ 0.0001. Quantification of enamel volume (c) and density (d) in the incisor, performed using Analyze 14.0 software. Statistical tests using One-Way ANOVA were performed for this analysis (n = 4 per group). ****$p < 0.0001$. Density was quantified in mg/cm³ of hydroxyapatite by converting Hounsfield Units (n = 4 mice per group).

**Fig. 3** Quantification of enamel volume (a) and density (b) in the first molar of WT mice, *G542X*, *G542X* Control ASO, and *G542X Ano1* ASO, aged 2-3 months and 4-6 months, performed using Analyze 14.0 software. Statistical tests using Two-way ANOVA were performed for this analysis (n = 4 per group). ****$p < 0.0001$; ***$p < 0.001$; **$p < 0.01$; *$p <$ 0.05; NS = Not Significant. Density was quantified in mg/cm³ of hydroxyapatite by converting Hounsfield Units. Quantification of hardness and elastic modulus of incisor (c) and molar (d) of WT mice, *G542X*, *G542X Ano1* ASO-treated or control ASO, aged 2 to 3 months, performed using Anton Paar indentation analysis software 9.0.11. 10 to 15 indents per tooth were made over the entire enamel surface to a depth of 3 µm. Statistical tests using One-way ANOVA were performed as part of this analysis (n = 3 mice per group). ****$p < 0.0001$; **$p < 0.01$; HIT: Hardness Indentation Test; EIT: Elasticity Indentation Test.

**Fig. 4** Scanning Electron Microscopy (SEM) characterization of enamel structure in WT, *G542X*, *G542X* Control ASO, and *G542X Ano1* ASO mice, aged 2-3 months. (a) Representative images of the enamel structure of the continuously growing incisor. Scale bars: 150 µm (overview) and 50 µm (zoomed-in region). (b) Representative images of molar enamel structure (first mesial root of M1) (n = 3 mice per group). Scale bars: 300 µm, 150 µm, and 50 µm. Red arrows indicate fractured prisms.

**Fig. 5** Enamel mineralization and ameloblast morphology in WT and *G542X* mice. (a) Incisor enamel mineralization and ameloblast morphology visualized using TC-CReM in WT, *G542X*, *G542X* Control ASO, and *G542X Ano1* ASO mice, aged 2–3 months. (b) First molar enamel mineralization was visualized using the same imaging technique in the same experimental groups. Images were acquired at 63× magnification with a section thickness of 50 µm and a z-step interval of 0.5 µm. Scale bars: 50 µm (n = 3 mice per group).

**Fig. 6** Expression patterns of *Ano1* and *Cftr* in ameloblasts. (a) Single-cell RNA-seq data from the previously established transcriptomic atlas of mouse tooth epithelium (Hermans et al.) was used to compare *Ano1* and *Cftr* expression across ameloblast populations. UMAP plots show normalized expressions of *Cftr* and *Ano1*. Both genes are expressed in pre-ameloblasts and

show differential expression in secretory-stage (sAB) and maturation-stage ameloblasts (mAB). Abbreviations: DEP: dental epithelial progenitors; IEE/OEE: inner/outer enamel epithelium; mAB: maturation-stage ameloblasts; preAB: pre-ameloblasts; sAB: secretory-stage ameloblasts; SI: stratum intermedium; SR: stellate reticulum; VEE/OEE: ventral/outer enamel epithelium. (b) RT-qPCR presenting the relative expression of *Cftr* and *Ano1* normalized to the reference gene *Gapdh* in salivary gland, sAB and mAB isolated from the incisor of WT mice aged 2–3 months. Statistical tests using One-Way ANOVA were performed for this analysis. ***$p < 0.001$; *$p < 0.05$ (c) Immunohistochemical staining using an anti-ANO1 antibody showing ANO1 expression in sAB and mAB of mouse incisors from WT mice aged 2–3 months. Lungs were used as a positive control for ANO1 staining (n = 3 WT mice) (Supplementary Material 2).

## Statements and Declarations

### Ethics approval

All animal experiments were approved by the Charles Darwin Ethical Committee (protocol numbers 38427-2022091211033928 v8 and 43883-2023062011193610 v7).


### Funding

Université Paris Cité founded this study. *In vivo* imaging was performed at the Life Imaging Facility of Paris Cité University (Plateforme Imageries du Vivant at the Micro-CT platform), supported by France Life Imaging (grant ANR-11-INBS-0006) and Infrastructures Biologie-Santé. This work was supported by grants from the University Paris Cité, Fondation de la Recherche Médicale (Grant DBS20131128438), Fondation des Gueules Cassées for INSERM UMR_S 1333 Oral Health. This project was partially founded by Blanche pour Vaincre la Mucoviscidose, Vaincre la Mucoviscidose, Fondation Maladies Rares, Anoat Therapeutics, Les Motards du Viaduc de Millau, and Inserm Transfert.

FH was supported by the Fund for Scientific Research (FWO) - Flanders (Belgium) (grant number 1226325N). Computational resources for all single cell transcriptome analyses were provided by the 'Vlaams Supercomputer Centrum' (VSC), managed by the Fund for Scientific Research (FWO) - Flanders (Belgium).


### Competing interests

The authors declare no competing interests.

**Authors' Contributions**

- **Dinne NEDJAR**: Drafted the manuscript with assistance from Dr. Françoise Tilotta, Dr. Olivier Tabary, Prof. Catherine Chaussain, and Dr. Christie Mitri. Performed macroscopic photography, micro-CT, nanoindentation, and immunohistochemistry experiments. Assisted Dr. The Nghia NGUYEN and Dr. Olivier Tabary with RT-qPCR.
- **Pr. Catherine Chaussain:** Contributed to the majority of the discussion section and oversaw the organization of all experimental procedures for the article.
- **Dr. Arnaud Vanden Bossche**: Conducted TC-CReM experiments with **Pr. Hubert Marotte**. Revised the Results and Materials and Methods sections related to these experiments.
- **Dr. Christie Mitri**: Assisted Dinne NEDJAR with manuscript drafting and revised the Introduction section.
- **Dr. The Nghia NGUYEN**: Conducted RT-qPCR experiments with Dr. Olivier Tabary. Revised the Materials and Methods section and the Results section related to RT-qPCR and immunohistochemistry.
- **Dr. Florian Hermans**: Performed transcriptomic analyses using RNA-seq. Revised the corresponding Materials and Methods and Results sections.
- **Dr. Nicolas Roubier** and **Dr. Elsa Vennat**: Revised the nanoindentation sections in Materials and Methods and Results. Assisted Dinne NEDJAR with nanoindentation experiments.
- **Dr. David Montero**: Conducted SEM experiments. Revised the associated Materials and Methods and Results sections.
- **Dr. Lotfi Slimani**: Revised the Micro-CT sections in Materials and Methods and Results. Assisted Dinne NEDJAR with image acquisition and segmentation in Micro-CT, also with the support of Dr. Françoise Tilotta.
- **Coralie TORRENS**: Prepared lung sections and performed immunohistochemistry for the positive control of the anti-ANO1 antibody.

**Acknowledgements**

*F508del* mice were generated by the CF EMCs (Dr. Scholte *et al.*) and the sponsorship of the EUROCARECF ($6^{th}$ framework coordination action program LSHM-CT-2005-018932).

*G542X* mice were generated by the CF Mouse Resource Center at Case Western Reserve University in the USA (Dr. Craig A. Hodges).

Arnaud Vanden-Bossche thanks INSERM and Jean Monnet University Saint-Etienne for their intramural funding of the SAINBIOSE U 1059 laboratory, as well as Alain Guignandon, Carl Zeiss SAS Research Microscopy Solution and Leslie Bancel-Vallée for their support.

The Federation of Chemistry and Materials of Paris-Center (UAR 2482) is acknowledged for access to SEM facilities, which were funded by Sorbonne Université, CNRS, and Région Ile de France.

**References**

[1] Mitri C, Xu Z, Bardin P, Corvol H, Touqui L, Tabary O. Novel Anti-Inflammatory Approaches for Cystic Fibrosis Lung Disease: Identification of Molecular Targets and Design of Innovative Therapies. Front Pharmacol. 23 juill 2020;11:1096. DOI: https://doi.org/10.3389/fphar.2020.01096

[2] Riordan JR, Rommens JM, Kerem BS, Alon N, Rozmahel R, Grzelczak Z, et al. Identification of the Cystic Fibrosis Gene: Cloning and Characterization of Complementary DNA. 245. DOI: https://doi.org/10.1126/science.2475911

[3] Elborn JS. Cystic fibrosis. The Lancet. nov 2016;388(10059):2519-31. DOI: https://doi.org/10.1016/s0140-6736(16)00576-6

[4] Goldberg JB, Hancock REW, Parales RE, Loper J, Cornelis P. Pseudomonas 2007. J Bacteriol. 2008;190:2649 62. DOI: https://doi.org/10.1128/jb.01950-07

[5] Elborn JS. Treatment of Staphylococcus aureus in cystic fibrosis. Thorax. 1999;54:377–8. DOI: https://doi.org/10.1136/thx.54.5.377

[6] Starner TD, Zhang N, Kim G, Apicella MA, McCray PB. Haemophilus influenzae Forms Biofilms on Airway Epithelia: Implications in Cystic Fibrosis. Am J Respir Crit Care Med. 2006;174:213–20. DOI: https://doi.org/10.1164/rccm.200509-1459oc

[7] Férec C. La mucoviscidose: Du gène à la thérapeutique. Med Sci (Paris). juin 2021;37(6-7):618-24. DOI: https://doi.org/10.1051/medsci/2021085

[8] Wang X, Li C. Decoding *F508del* Misfolding in Cystic Fibrosis. Biomolecules. 6 mai 2014;4(2):498-509. DOI: https://doi.org/10.3390/biom4020498

[9] Sharma J, Abbott J, Klaskala L, Zhao G, Birket SE, Rowe SM. A Novel *G542X* CFTR Rat Model of Cystic Fibrosis Is Sensitive to Nonsense Mediated Decay. Front Physiol. 16 déc 2020;11:611294. DOI: https://doi.org/10.3389/fphys.2020.611294

[10] Arquitt CK, Boyd C, Wright JT. Cystic Fibrosis Transmembrane Regulator Gene (CFTR) is Associated with Abnormal Enamel Formation. J Dent Res. juill 2002;81(7):492-6. DOI: https://doi.org/10.1177/154405910208100712

[11] Peker S, Mete S, Gokdemir Y, Karadag B, Kargul B. Related factors of dental caries and molar incisor hypomineralisation in a group of children with cystic fibrosis. Eur Arch Paediatr Dent. août 2014;15(4):275-80. DOI: https://doi.org/10.1007/s40368-014-0112-5

[12] O'Leary F, Coffey N, Hayes M, Burke F, Harding M, Plant B. The prevalence of developmental defects of enamel in people with cystic fibrosis: a systematic review. BMC Oral Health. 12 avr 2024;24(1):446. DOI: https://doi.org/10.1186/s12903-024-04227-4

[13] Wright JT, Kiefer CL, Hall KI, Grubb BR. Abnormal Enamel Development in a Cystic Fibrosis Transgenic Mouse Model. J Dent Res. avr 1996;75(4):966-73. DOI: https://doi.org/10.1177/00220345960750041101

[14] Wright JT, Hall KI, Grubb BR. Enamel Mineral Composition of Normal and Cystic Fibrosis Transgenic Mice. Adv Dent Res. nov 1996;10(2):270-5. DOI: https://doi.org/10.1177/08959374960100022501

[15] Chang EH, Lacruz RS, Bromage TG, Bringas, Jr. P, Welsh MJ, Zabner J, et al. Enamel Pathology Resulting from Loss of Function in the Cystic Fibrosis Transmembrane Conductance Regulator in a Porcine Animal Model. Cells Tissues Organs. 2011;194(2-4):249-54. DOI: https://doi.org/10.1159/000324248

[16] Bronckers ALJJ, Lyaruu DM, Guo J, Bijvelds MJC, Bervoets TJM, Zandieh-Doulabi B, et al. Composition of mineralizing incisor enamel in cystic fibrosis transmembrane conductance regulator-deficient mice. European J Oral Sciences. févr 2015;123(1):9-16. DOI: https://doi.org/10.1111/eos.12163

[17] Dreano E, Bacchetta M, Simonin J, Galmiche L, Usal C, Slimani L, et al. Characterization of two rat models of cystic fibrosis—KO and *F508del* CFTR—Generated by Crispr-Cas9. Anim Models and Exp Med. déc 2019;2(4):297-311. DOI: https://doi.org/10.1002/ame2.12091

[18] Lacruz RS, Habelitz S, Wright JT, Paine ML. Dental Enamel Formation and Implications for Oral Health and Disease. Physiological Reviews. 1 juill 2017;97(3):939-93. DOI: https://doi.org/10.1152/physrev.00030.2016

[19] Bronckers A, Kalogeraki L, Jorna HJN, Wilke M, Bervoets TJ, Lyaruu DM, et al. The cystic fibrosis transmembrane conductance regulator (CFTR) is expressed in maturation stage ameloblasts, odontoblasts and bone cells. Bone. avr 2010;46(4):1188-96. DOI: https://doi.org/10.1016/j.bone.2009.12.002

[20] Sui W, Boyd C, Wright JT. Altered pH Regulation During Enamel Development in the Cystic Fibrosis Mouse Incisor. J Dent Res. mai 2003;82(5):388-92. DOI: 10.1177/154405910308200512

[21] Yin K, Paine ML. Bicarbonate Transport During Enamel Maturation. Calcif Tissue Int. nov 2017;101(5):457-64. DOI: https://doi.org/10.1177/154405910308200512

[22] Pawlaczyk-Kamieńska T, Borysewicz-Lewicka M, Śniatała R, Batura-Gabryel H, Cofta S. Dental and periodontal manifestations in patients with cystic fibrosis - A systematic review. Journal of Cystic Fibrosis. nov 2019;18(6):762-71. DOI: https://doi.org/10.1016/j.jcf.2018.11.007

[23] Graeber SY, Mall MA. The future of cystic fibrosis treatment: from disease mechanisms to novel therapeutic approaches. The Lancet. 30 sept 2023;402(10408):1185-98. DOI: https://doi.org/10.1016/S0140-6736(23)01608-2

[24] Allen L, Allen L, Carr SB, Davies G, Downey D, Egan M, et al. Future therapies for cystic fibrosis. Nat Commun. 8 févr 2023;14(1):693. DOI: https://doi.org/10.1038/s41467-023-36244-2

[25] Sonneville F, Ruffin M, Coraux C, Rousselet N, Le Rouzic P, Blouquit-Laye S, et al. MicroRNA 9 downregulates the ANO1 chloride channel and contributes to cystic fibrosis lung pathology. Nat Commun. 27 sept 2017;8(1):710. DOI: https://doi.org/10.1038/s41467-017-00813-z

[26] Schroeder BC, Cheng T, Jan YN, Jan LY. Expression Cloning of ANO1 as a Calcium Activated Chloride Channel Subunit. Cell. sept 2008;134(6):1019-29. DOI: https://doi.org/10.1016/j.cell.2008.09.003

[27] Yang YD, Cho H, Koo JY, Tak MH, Cho Y, Shim WS, et al. ANO1 confers receptor activated calcium-dependent chloride conductance. Nature. oct 2008;455(7217):1210-5. DOI: https://doi.org/10.1038/nature07313

[28] Caputo A, Caci E, Ferrera L, Pedemonte N, Barsanti C, Sondo E, et al. ANO1, A Membrane Protein Associated with Calcium-Dependent Chloride Channel Activity. Science. 24 oct 2008;322(5901):590-4. DOI: https://doi.org/10.1126/science.1163518

[29] Jia L, Liu W, Guan L, Lu M, Wang K. Inhibition of Calcium-Activated Chloride Channel ANO1/TMEM16A Suppresses Tumor Growth and Invasion in Human Lung Cancer. Xu SZ, éditeur. PLoS ONE. 25 août 2015;10(8):e0136584. DOI: https://doi.org/10.1371/journal.pone.0136584

[30] Jung J, Nam JH, Park HW, Oh U, Yoon JH, Lee MG. Dynamic modulation of ANO1/ TMEM16A HCO 3 − permeability by Ca 2+ /calmodulin. Proc Natl Acad Sci USA. 2 janv 2013;110(1):360-5. DOI: https://doi.org/10.1073/pnas.1211594110

[31] Mitri C, Sharma H, Corvol H, Tabary O. TMEM16A /ANO1: Current Strategies and Novel Drug Approaches for Cystic Fibrosis. Cells. 24 oct 2021;10(11):2867. 10.3390/cells10112867 DOI: https://doi.org/10.3390/cells10112867

[32] Ruffin M, Voland M, Marie S, Bonora M, Blanchard E, Blouquit-Laye S, et al. Anoctamin 1 dysregulation alters bronchial epithelial repair in cystic fibrosis. Biochimica et Biophysica Acta (BBA) - Molecular Basis of Disease. déc 2013;1832(12):2340-51. DOI: https://doi.org/10.1016/j.bbadis.2013.09.012

[33] Dai W, Qiu J, Sun J, Ma C, Huang N, Jiang Y, et al. Downregulation of microRNA-9 reduces inflammatory response and fibroblast proliferation in mice with idiopathic pulmonary fibrosis through the ANO1-mediated TGF-β–Smad3 pathway. Journal Cellular Physiology. mars 2019;234(3):2552-65. DOI: https://doi.org/10.1002/jcp.26961

[34] Park YR, Lee ST, Kim SL, Zhu SM, Lee MR, Kim SH, et al. Down-regulation of miR-9 promotes epithelial mesenchymal transition via regulating anoctamin-1 (ANO1) in CRC cells. Cancer Genetics. févr 2019;231-232:22-31. DOI: https://doi.org/10.1016/j.cancergen.2018.12.004

[35] Mitri C. Development of an RNA therapy : a new approach to treat all cystic fibrosis patients with antisense oligonucleotide. 2022.

[36] Mitri C, Rousselet N, Bardin P, Wickramanayaka MD, Foussignière T, Dupuis G, et al. Restoring Chloride Efflux in Cystic Fibrosis with TMEM16a Antisense Oligonucleotides. Molecular Therapy. sept 2025;S1525001625007191. DOI: https://doi.org/10.1016/j.ymthe.2025.08.045

[37] Pharr GM, Oliver WC, Brotzen FR. On the generality of the relationship among contact stiffness, contact area, and elastic modulus during indentation. J Mater Res. mars 1992;7(3):613-7. DOI: https://doi.org/10.1557/JMR.1992.0613

[38] Dent JA, Polson AG, Klymkowsky MW. A whole-mount immunocytochemical analysis of the expression of the intermediate filament protein vimentin in Xenopus. Development. 1 janv 1989;105(1):61-74. DOI: https://doi.org/10.1242/dev.105.1.61

[39] Hermans F, Bueds C, Hemeryck L, Lambrichts I, Bronckaers A, Vankelecom H. Establishment of inclusive single-cell transcriptome atlases from mouse and human tooth as powerful resource for dental research. Front Cell Dev Biol. 10 oct 2022;10:1021459. DOI: https://doi.org/10.3389/fcell.2022.1021459

[40] Young MD, Behjati S. SoupX removes ambient RNA contamination from droplet-based single-cell RNA sequencing data. GigaScience. 26 déc 2020;9(12):giaa151. DOI: https://doi.org/10.1093/gigascience/giaa151

[41] Hao Y, Hao S, Andersen-Nissen E, Mauck WM, Zheng S, Butler A, et al. Integrated analysis of multimodal single-cell data. Cell. juin 2021;184(13):3573-3587.e29. DOI: https://doi.org/10.1016/j.cell.2021.04.048

[42] Houari S, Babajko S, Loiodice S, Berdal A, Jedeon K. Micro-dissection of Enamel Organ from Mandibular Incisor of Rats Exposed to Environmental Toxicants. JoVE. 29 mars 2018;(133):57081. DOI: https://dx.doi.org/10.3791/57081

[43] Srot V, Houari S, Kapun G, Bussmann B, Predel F, Pokorny B, et al. Ingenious Architecture and Coloration Generation in Enamel of Rodent Teeth. ACS Nano. 30 avr 2024;18(17):11270-83. DOI: https://doi.org/10.1021/acsnano.4c00578

[44] Tuggle KL, Birket SE, Cui X, Hong J, Warren J, Reid L, et al. Characterization of Defects in Ion Transport and Tissue Development in Cystic Fibrosis Transmembrane Conductance Regulator (CFTR)-Knockout Rats. Boyaka PN, éditeur. PLoS ONE. 7 mars 2014;9(3):e91253. DOI: https://doi.org/10.1371/journal.pone.0091253

[45] Catalán MA, Scott-Anne K, Klein MI, Koo H, Bowen WH, Melvin JE. Elevated Incidence of Dental Caries in a Mouse Model of Cystic Fibrosis. Semple M, éditeur. PLoS ONE. 31 janv 2011;6(1):e16549. DOI: https://doi.org/10.1371/journal.pone.0091253

[46] Yu T, Klein OD. Molecular and cellular mechanisms of tooth development, homeostasis and repair. Development [Internet]. 15 janv 2020 [cité 22 juill 2025];147(2). doi: https://doi.org/10.1242/dev.184754

[47] Smith CE, Bartlett JD, Simmer JP, Hu JCC. Challenges of Studying Amelogenesis in Gene-Targeted Mouse Models. IJMS. 20 mai 2025;26(10):4905. DOI: https://doi.org/10.3390/ijms26104905

[48] Smith CEL, Poulter JA, Antanaviciute A, Kirkham J, Brookes SJ, Inglehearn CF, et al. Amelogenesis Imperfecta; Genes, Proteins, and Pathways. Front Physiol [Internet]. 26 juin 2017 [cité 22 juill 2025];8. DOI: https://doi.org/10.3389/fphys.2017.00435

[49] Schreiber R, Ousingsawat J, Kunzelmann K. Epithelial Anoctamins. Cell Calcium. 1 juin 2024;120:102885. DOI: https://doi.org/10.3389/fphys.2017.00435

[50] Shin Y, Lee SW, Namkoong E, An W, Lee JH, Brown PD, et al. Epigenetic Modification as a Regulatory Mechanism for Spatiotemporal Dynamics of ANO1 Expression in Salivary Glands. IJMS. 13 déc 2019;20(24):6298. DOI: https://doi.org/10.3390/ijms20246298

[51] Ko D (Jihyung), Kelly T, Thompson L, Uppal JK, Rostampour N, Webb MA, et al. Timing of Mouse Molar Formation Is Independent of Jaw Length Including Retromolar Space. JDB. 12 mars 2021;9(1):8. DOI: https://doi.org/10.3390/jdb9010008

[52] Shcheynikov N, Kim KH, Kim K mi, Dorwart MR, Ko SBH, Goto H, et al. Dynamic Control of Cystic Fibrosis Transmembrane Conductance Regulator C l − / H C O 3 − Selectivity by External Cl–. Journal of Biological Chemistry. mai 2004;279(21):21857-65. DOI: https://doi.org/10.1074/jbc.M313323200

[53] Abreu De Moraes D, Negrini Lia É, Jácome LMT, De Azevedo Pedrosa Cunha C, De Freitas Velloso Monte L. Oral health in individuals with cystic fibrosis: A cross-sectional study. Heliyon. févr 2024;10(3):e25241. DOI: https://doi.org/10.1016/j.heliyon.2024.e25241

[54] Kunzelmann K, Schreiber R, Hadorn HB. Bicarbonate in cystic fibrosis. Journal of Cystic Fibrosis. nov 2017;16(6):653-62. DOI: https://doi.org/10.1016/j.jcf.2017.06.005

[55] Muñoz M, Acevedo A, Ovitt CE, Luitje ME, Maruyama EO, Catalán MA. CFTR expression in human salivary gland acinar cells. American Journal of Physiology-Cell Physiology. 1 mars 2024;326(3):C742-8. DOI : https://doi.org/10.1152/ajpcell.00549.2023

[56] Catalán MA, Nakamoto T, Gonzalez-Begne M, Camden JM, Wall SM, Clarke LL, et al. Cftr and ENaC ion channels mediate NaCl absorption in the mouse submandibular gland: Functional interplay between Cftr and ENaC. The Journal of Physiology. 15 févr 2010;588(4):713-24. DOI: https://doi.org/10.1113/jphysiol.2009.183541

[57] Yin K, Lei Y, Wen X, Lacruz RS, Soleimani M, Kurtz I, et al. SLC26A Gene Family Participate in pH Regulation during Enamel Maturation. Matsumoto T, éditeur. PLoS ONE. 15 déc 2015;10(12):e0144703. DOI: https://doi.org/10.1371/journal.pone.0144703

[58] Hagan ML, Tuladhar A, Yu K, Alhamad DW, Bensreti H, Dorn J, et al. Osteocyte Sptbn1 Deficiency Alters Cell Survival and Mechanotransduction Following Formation of Plasma Membrane Disruptions (PMD) from Mechanical Loading. Calcified Tissue International. 1 nov 2024;115(5):725-43. DOI: https://doi.org/10.1016/j.cell.2021.04.048

[59] Tuladhar A, Guffroy M, Finnema SJ, Christmann R, Van Vleet TR, Mayana SAK, et al. Investigation of bone toxicity in drug development: review of current and emerging technologies. Toxicological Sciences. 26 sept 2025; kfaf131. DOI: https://doi.org/10.1093/toxsci/kfaf131

[60] Özçelik U, Beþbaþ N, Göçmen A, Akata D, Akhan O, Özgüç M, et al. Hypercalciuria and nephrocalcinosis in cystic fibrosis patients. The Turkish Journal of Pediatrics. 2004;46(1). PMID: https://turkjpediatr.org/article/view/2764/2722

[61] Yahiaoui Y, Jablonski M, Hubert D, Mosnier-Pudar H, Noe[Combining Diaeresis]l LHAAGA, Stern M, et al. Renal Involvement in Cystic Fibrosis: Diseases Spectrum and Clinical Relevance. Clinical Journal of the American Society of Nephrology. mai 2009;4(5):921-8. DOI: https://doi.org/10.2215/CJN.00750209

[62] Katz Sheila Moriber, Krueger Leslie J., Falkner Bonita. Microscopic Nephrocalcinosis in Cystic Fibrosis. New England Journal of Medicine. 4 août 1988;319(5):263-6. DOI: https://doi.org/10.1056/NEJM198808043190502

[63] Dif F, Marty C, Baudoin C, De Vernejoul MC, Levi G. Severe osteopenia in CFTR-null mice. Bone. sept 2004;35(3):595-603. DOI: https://doi.org/10.1016/j.bone.2004.05.021

[64] Kovacs CS, Chaussain C, Osdoby P, Brandi ML, Clarke B, Thakker RV. The role of biomineralization in disorders of skeletal development and tooth formation. Nat Rev Endocrinol. juin 2021;17(6):336-49. DOI: https://doi.org/10.1038/s41574-021-00488-z

[65] Bardet C, Courson F, Wu Y, Khaddam M, Salmon B, Ribes S, et al. Claudin-16 Deficiency Impairs Tight Junction Function in Ameloblasts, Leading to Abnormal Enamel Formation. Journal of Bone and Mineral Research. 1 mars 2016;31(3):498-513. DOI: https://doi.org/10.1002/jbmr.2726

[66] Bardet C, Ribes S, Wu Y, Diallo MT, Salmon B, Breiderhoff T, et al. Claudin Loss-of-Function Disrupts Tight Junctions and Impairs Amelogenesis. Front Physiol. 2017;8:326. DOI: https://doi.org/10.3389/fphys.2017.00326

[67] Yamaguti PM, Neves FDAR, Hotton D, Bardet C, De La Dure-Molla M, Castro LC, et al. Amelogenesis imperfecta in familial hypomagnesaemia and hypercalciuria with nephrocalcinosis caused by CLDN19 gene mutations. J Med Genet. 2017;54:26–37. DOI: https://doi.org/10.1136/jmedgenet-2016-103956

[68] Beniash E, Stifler CA, Sun CY, Jung GS, Qin Z, Buehler MJ, et al. The hidden structure of human enamel. Nat Commun [Internet]. 26 sept 2019 [cité 26 juill 2025];10(1). DOI: https://doi.org/10.1038/s41467-019-12185-7

# Figure 1

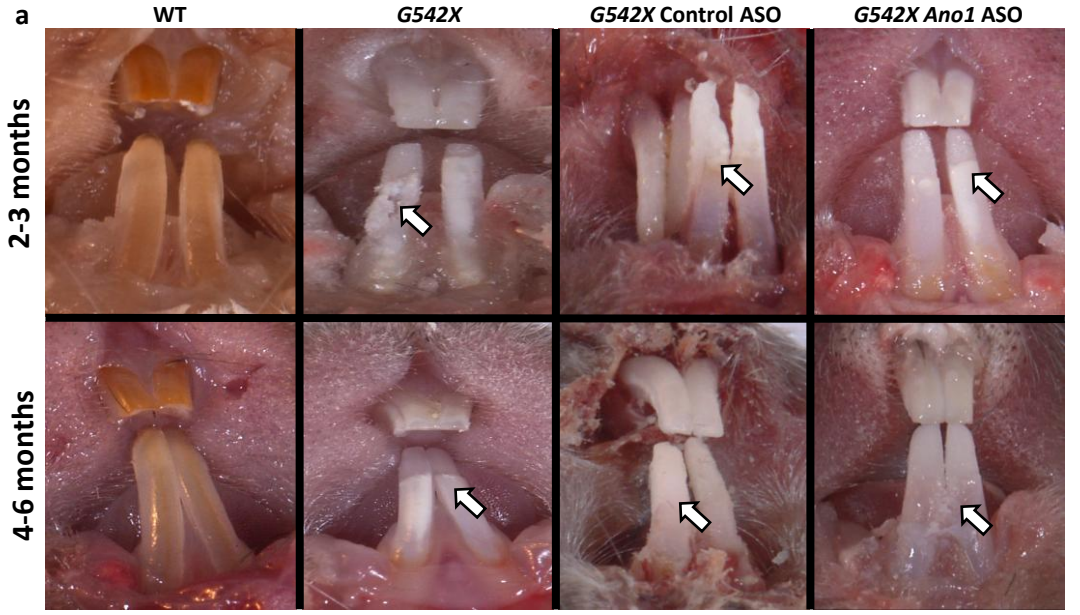
a
WT
G542X
G542X Control ASO
G542X Ano1 ASO
2-3 months
4-6 months

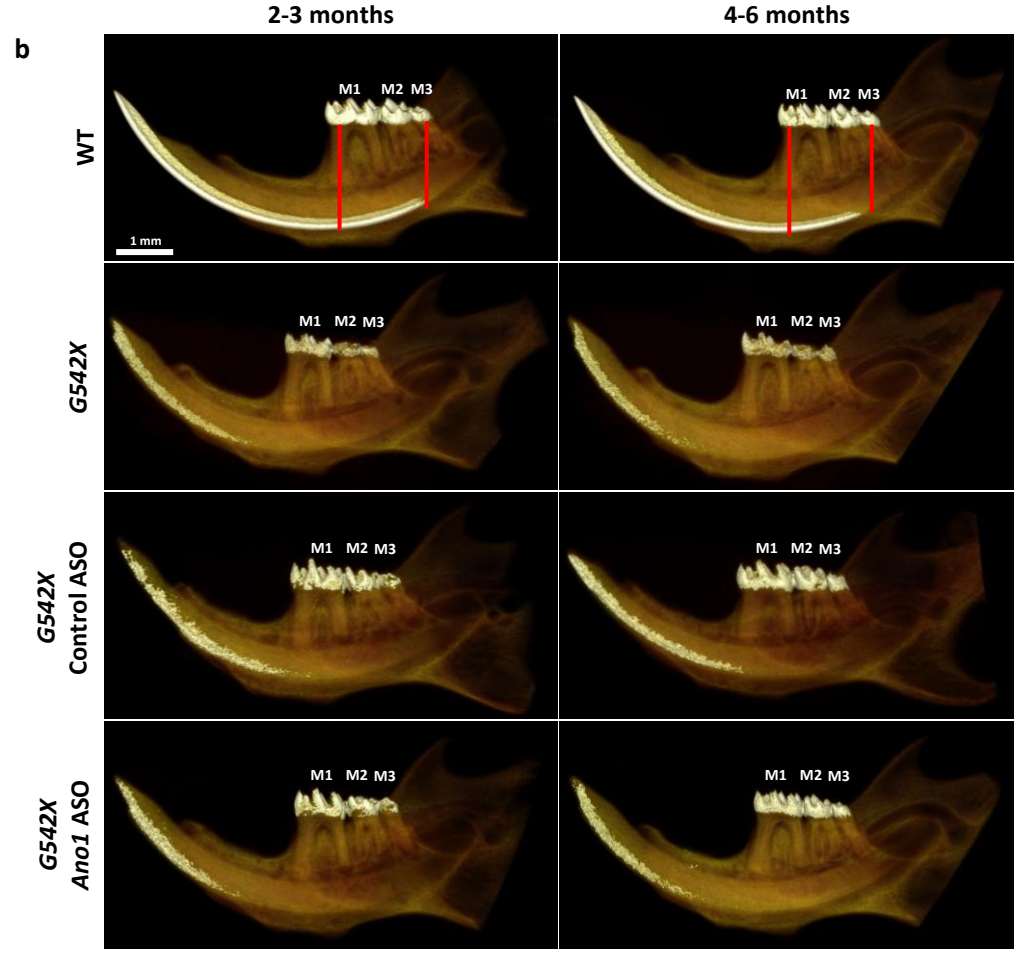
b
2-3 months
4-6 months
WT
G542X
G542X Control ASO
G542X Ano1 ASO
M1 M2 M3
1 mm

# Figure 2

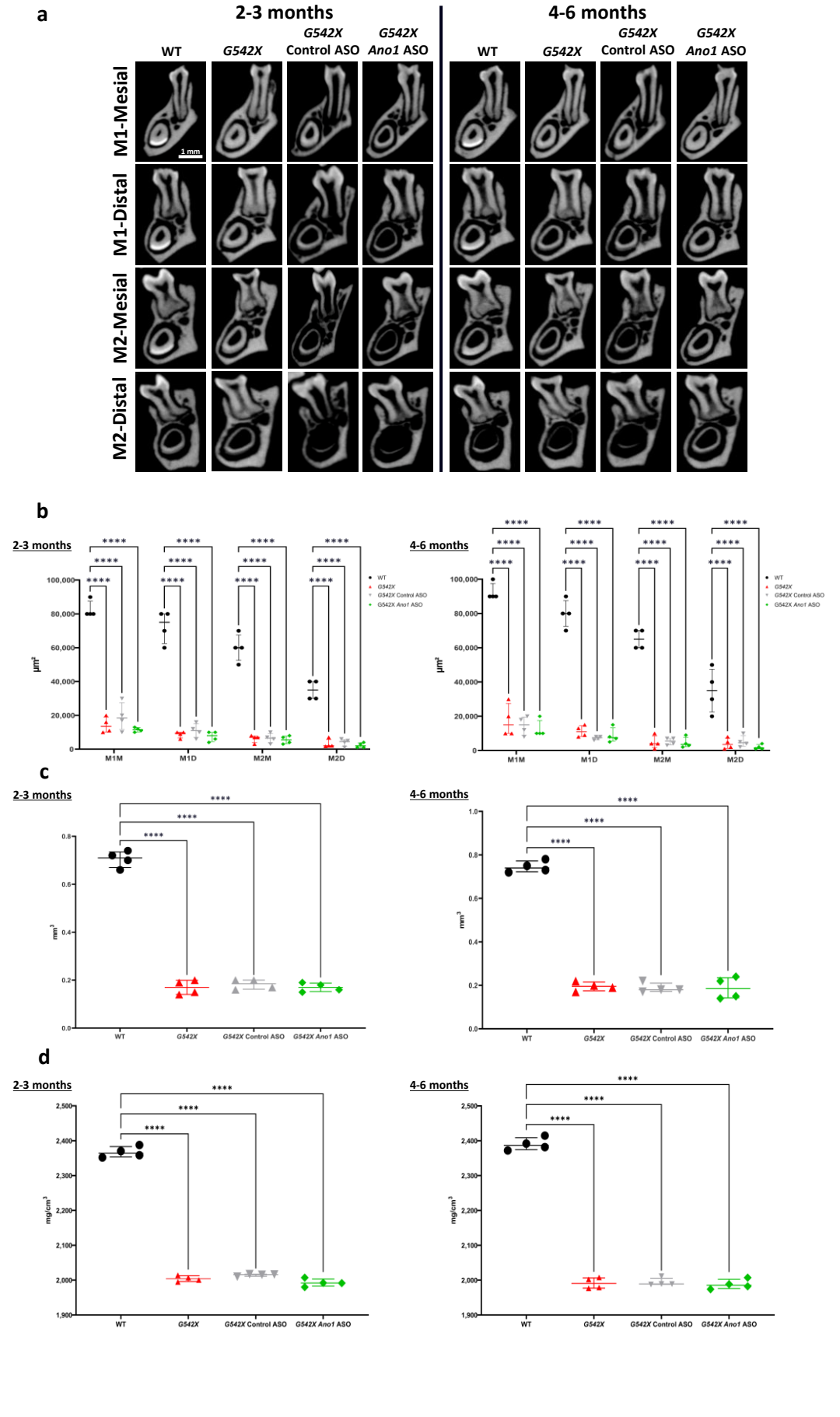
a
2-3 months
4-6 months
WT
G542X
G542X Control ASO
G542X Ano1 ASO
M1-Mesial
M1-Distal
M2-Mesial
M2-Distal
1 mm
b
2-3 months
4-6 months
µm³
M1M
M1D
M2M
M2D
****
c
2-3 months
4-6 months
mm³
d
2-3 months
4-6 months
mg/cm³

Figure 3

a Volume of enamel molar

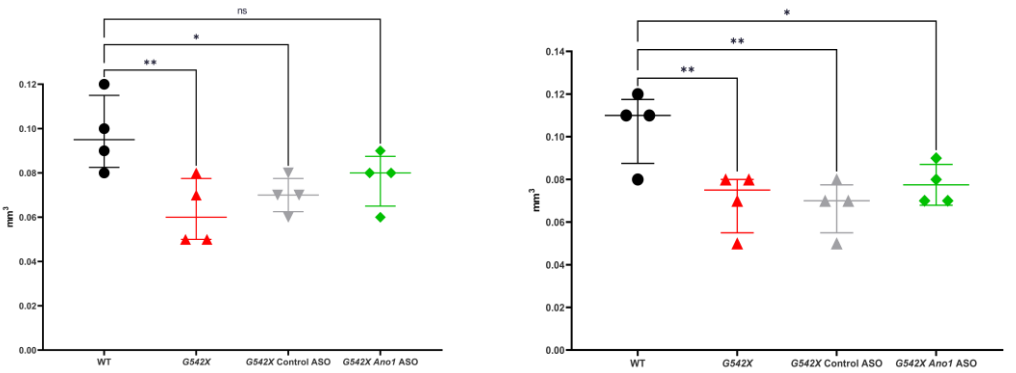


b Density of enamel molar

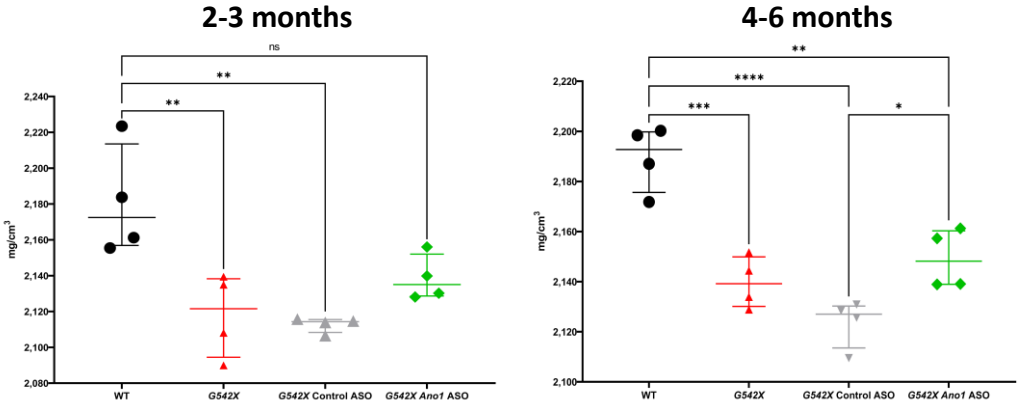


c Enamel incisor

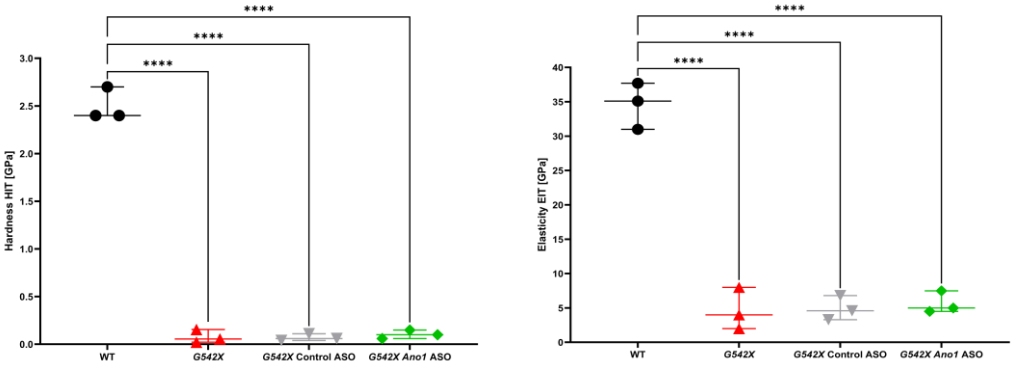


d Enamel molar

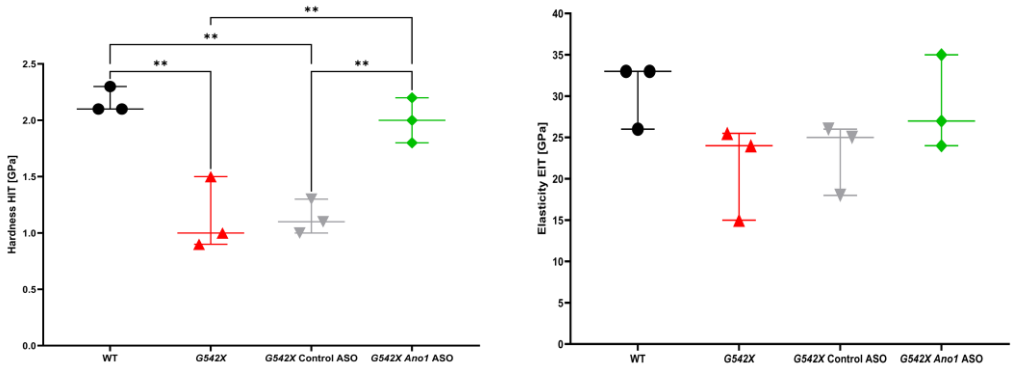

Figure 4

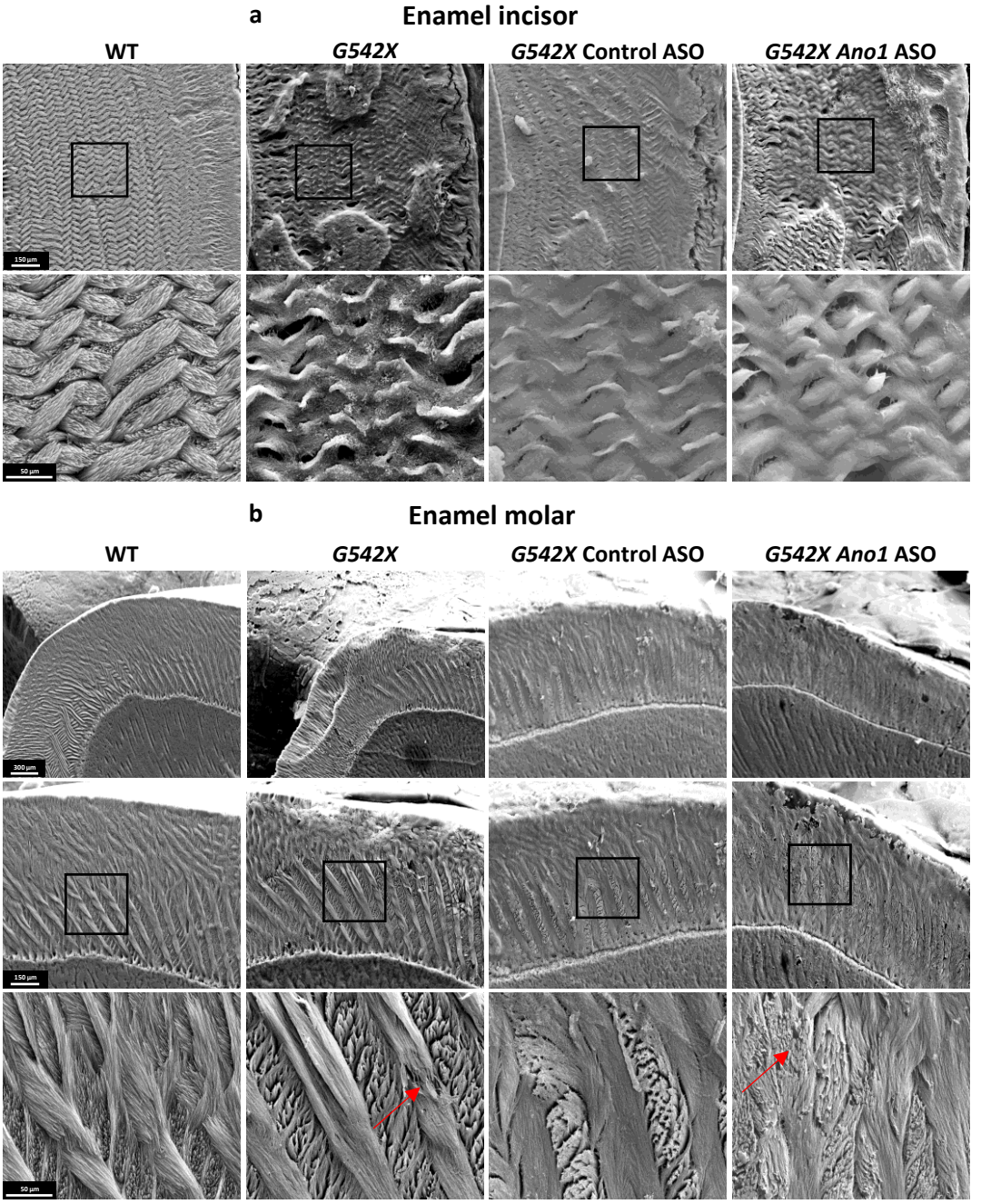
a
Enamel incisor
WT
G542X
G542X Control ASO
G542X Ano1 ASO
150 µm
50 µm
b
Enamel molar
WT
G542X
G542X Control ASO
G542X Ano1 ASO
300 µm
150 µm
50 µm

Figure 5

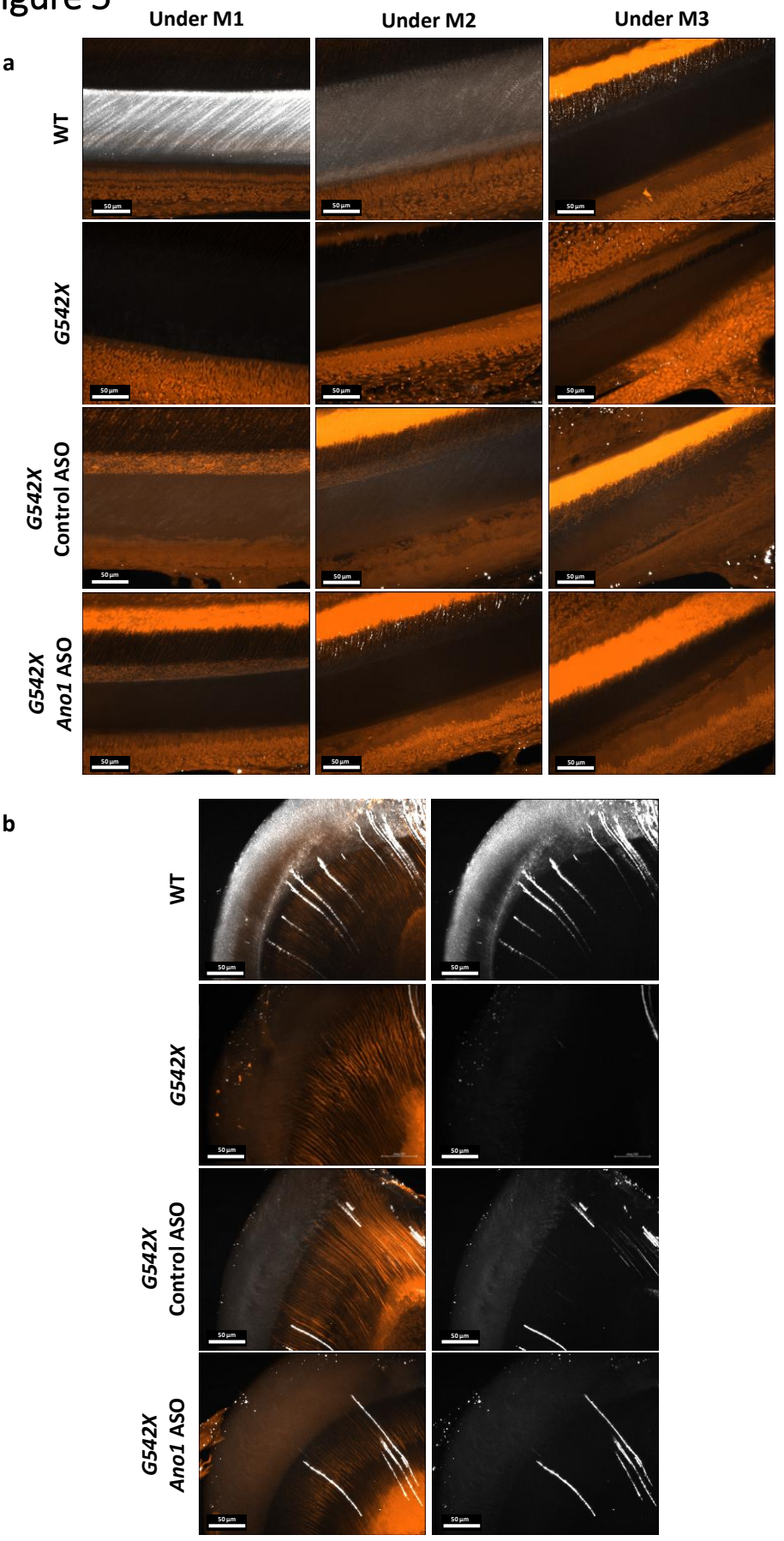
Under M1
Under M2
Under M3
a
WT
G542X
G542X Control ASO
G542X Ano1 ASO
50 µm
b
WT
G542X
G542X Control ASO
G542X Ano1 ASO
50 µm

# Figure 6

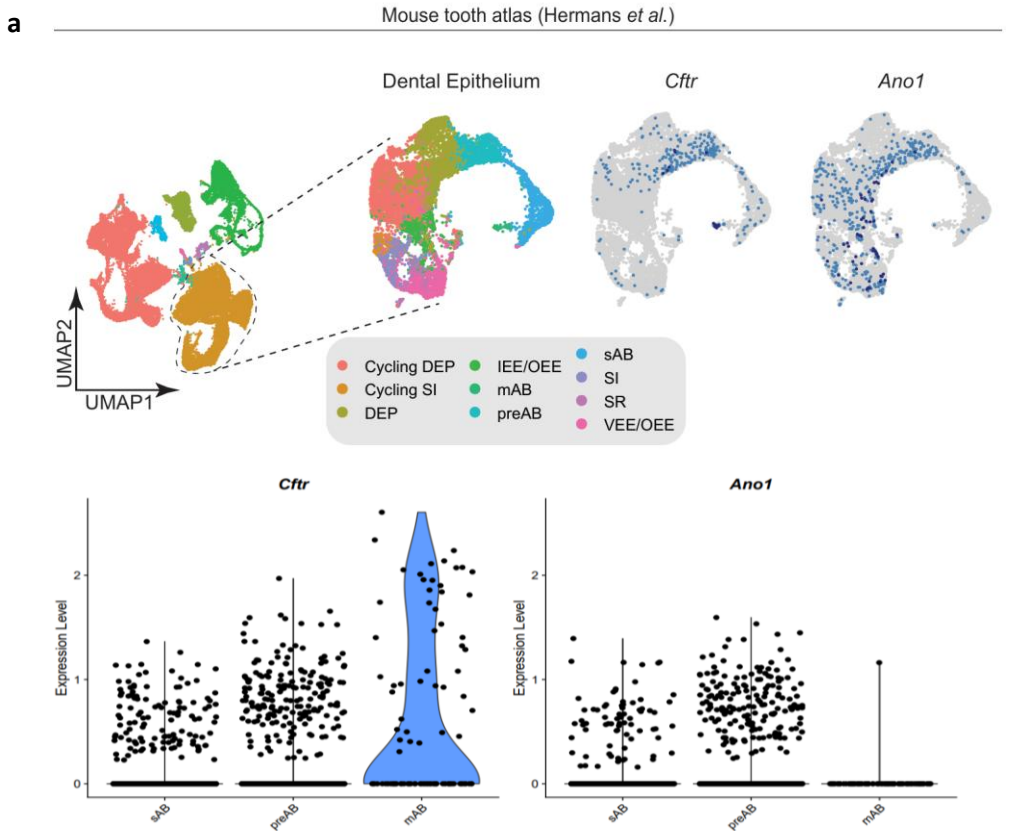
a
Mouse tooth atlas (Hermans et al.)
Dental Epithelium
Cftr
Ano1
UMAP2
UMAP1
Cycling DEP
Cycling SI
DEP
IEE/OEE
mAB
preAB
sAB
SI
SR
VEE/OEE
Cftr
Ano1
Expression Level
sAB
preAB
mAB

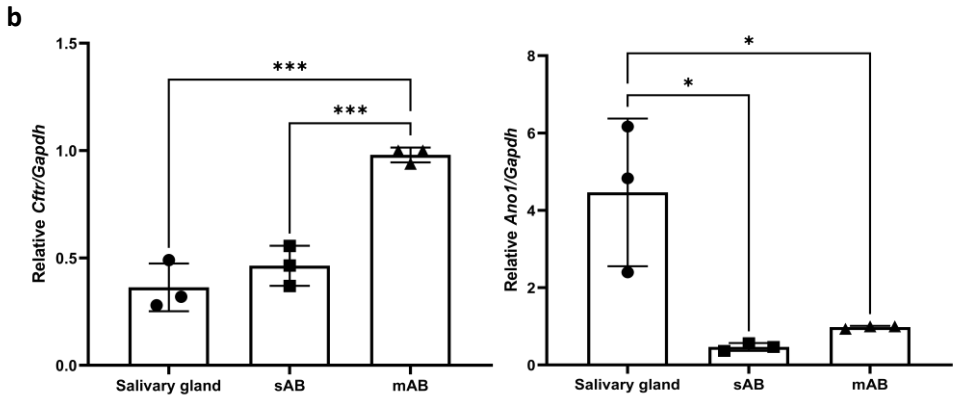
b
Relative Cftr/Gapdh
Relative Ano1/Gapdh
***
***
*
*
Salivary gland
sAB
mAB

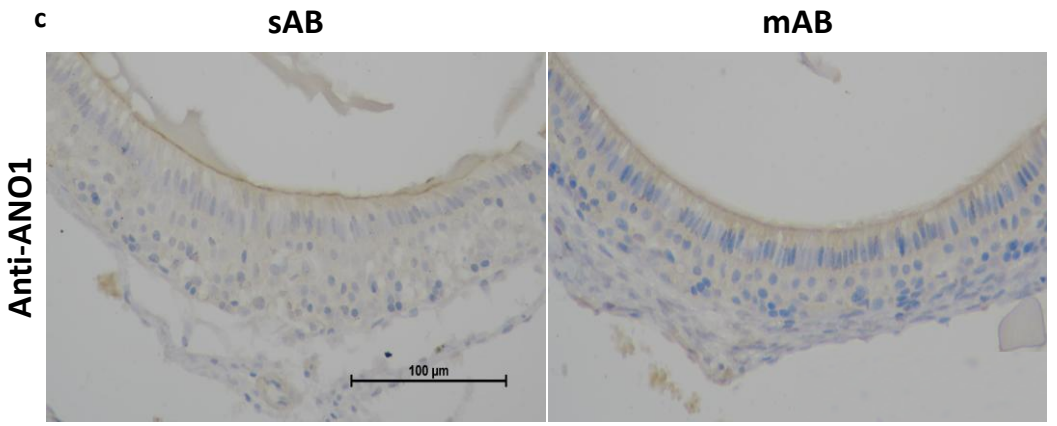
c
sAB
mAB
Anti-ANO1
100 μm

# Supplementary Material 1

Tissue Clearing and Confocal Reflexion Microscopy (TC-CReM)

The TC-CReM method originates from the combination of a biological tissue preparation technique and a microscopy imaging technique.

The first histological technique, dating back to the late 19th century, is tissue clearing, pioneered by the anatomist Werner Spalteholz. Since its inception, it has been repeatedly modified to accommodate different tissues and the evolving resolution of optical microscopes (DOI: 10.15252/msb.20209807). Today, it is commonly referred to as Tissue Clearing. The principle involves homogenizing the refractive index of the tissue to reduce light scattering and improve imaging quality. Its effectiveness depends on the heterogeneity of the tissues studied and the specific structures to be visualized. There is often a temptation to "over-clear" the tissue using pre-fixation followed by sequential chemical treatments such as decalcification, depigmentation or bleaching, delipidation, dehydration, degassing, and clearing. The goal is to achieve a homogeneous refractive index throughout the volume at all scales, facilitating access for various fluorescent probes and enhancing resolution. The advantage lies in optimizing optical conditions to observe the targeted information across a maximal volume (DOI: 10.1177/0022034519844510). However, excessive tissue processing may lead to the loss of unexpected information and potential serendipitous findings. Accordingly, the histological preparation for TC-CReM has been simplified, omitting decalcification.

The second imaging technique, developed in the second half of the 20th century, is Laser Scanning Confocal Microscopy (LSCM). Offering enhanced lateral and axial resolution within a volume, LSCM is designed for detecting fluorescence emitted by different fluorescent probes excited by a laser scan. It can also detect reflected light (DOI: 10.1385/MB:16:2:127).

Tissue Clearing for LSCM, Light Sheet microscopy (DOI: 10.1016/j.exer.2018.12.001), or multiphoton microscopy for volumetric fluorescence detection has generated an exponential number of publications over the past 50 years, with a peak of 4,529 articles indexed on PubMed in 2021 under "Tissue clearing." Now a standard approach in multiscale biology (DOI: 10.1038/s43586-021-00080-9), it provides improved understanding of three-dimensional tissue structures (DOI: 10.1242/dev.199369).

Surprisingly, Tissue Clearing for volumetric fluorescence imaging of cleared biological tissues has not been combined with reflection detection. We applied it to study enamel in correlation with other classical observation and quantification techniques for amelogenesis.

We demonstrated that Tissue Clearing and Confocal Reflection Microscopy (TC-CReM) enables the visualization of micrometer-sized fluorescent objects, such as cell nuclei, and nanometer-sized reflective objects, such as enamel crystals undergoing maturation, within the same cleared tissue volume. The histological procedure has been simplified, with minimal processing to preserve maximum information. No decalcification is performed after fixation; tissues are stained/dehydrated with rhodamine 6G–colored ethanol, rinsed under vacuum, and cleared using a benzyl benzoate and benzyl alcohol mixture.

The combined detection of fluorescence and reflection enables 3D imaging of cleared volumes containing fluorescent structures and reflective nano-objects, such as crystalline or metallic components and air interfaces. TC-CReM exploits both fluorescent and reflective signals to visualize internal structures, identify non-fluorescent features, and generate detailed 3D representations for in-depth analysis in an optically transparent environment.

# Supplementary Material 1

**a** **Technical principle of TC-CReM:**

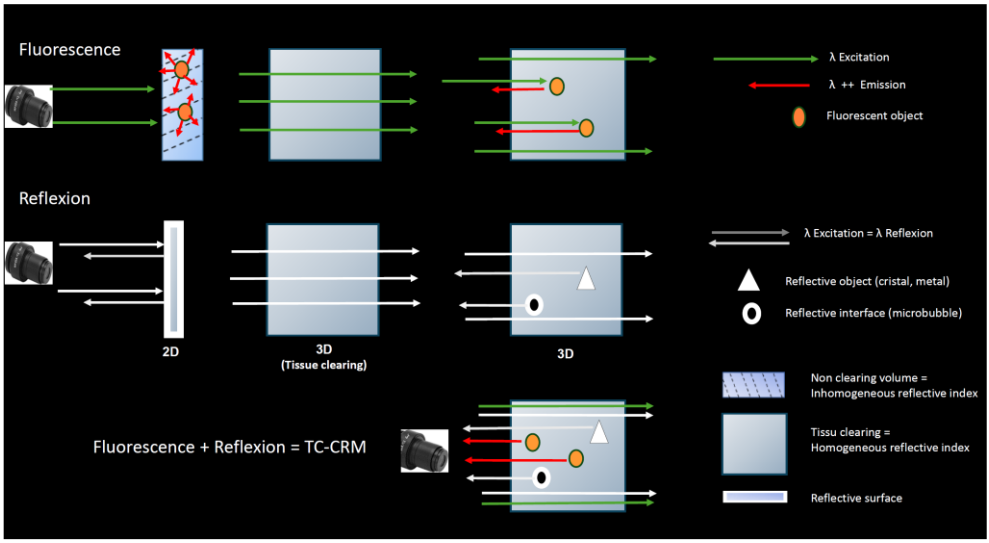


**b** **Optical principle of TC-CReM:**

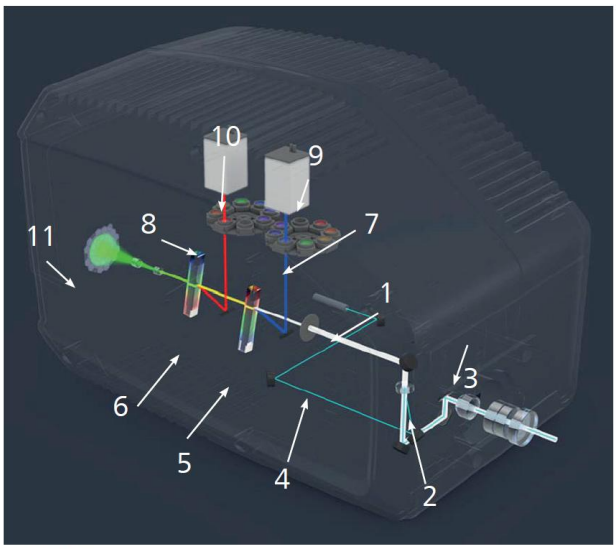


**LSM 800**

The LSM 800 system is commercially available from ZEISS. It includes a laser source configured to emit an excitation wavelength of 640 nm, used for both fluorescence and reflection, with identical laser power and variable gain settings.

The "VSD"1 component functions as a mirror, reflecting the 640 nm laser. The emission filter in front of the photomultiplier detector (PMT1) is removed to collect the full 640 nm reflection signal.

(1) Lasers
(2) Main Beam Splitter
(3) Scanners
(4) Pinhole
(5) Variable Secondary Dichroic "VSD" 1 (High-pass)
(6) Variable Secondary Dichroic "VSD" 2 (Low-pass)
(7) Emission filter for PMT1 (9)
(8)Emission filter for PMT3 (10)
(11) PMT2 or Airyscan

# Supplementary Material 2

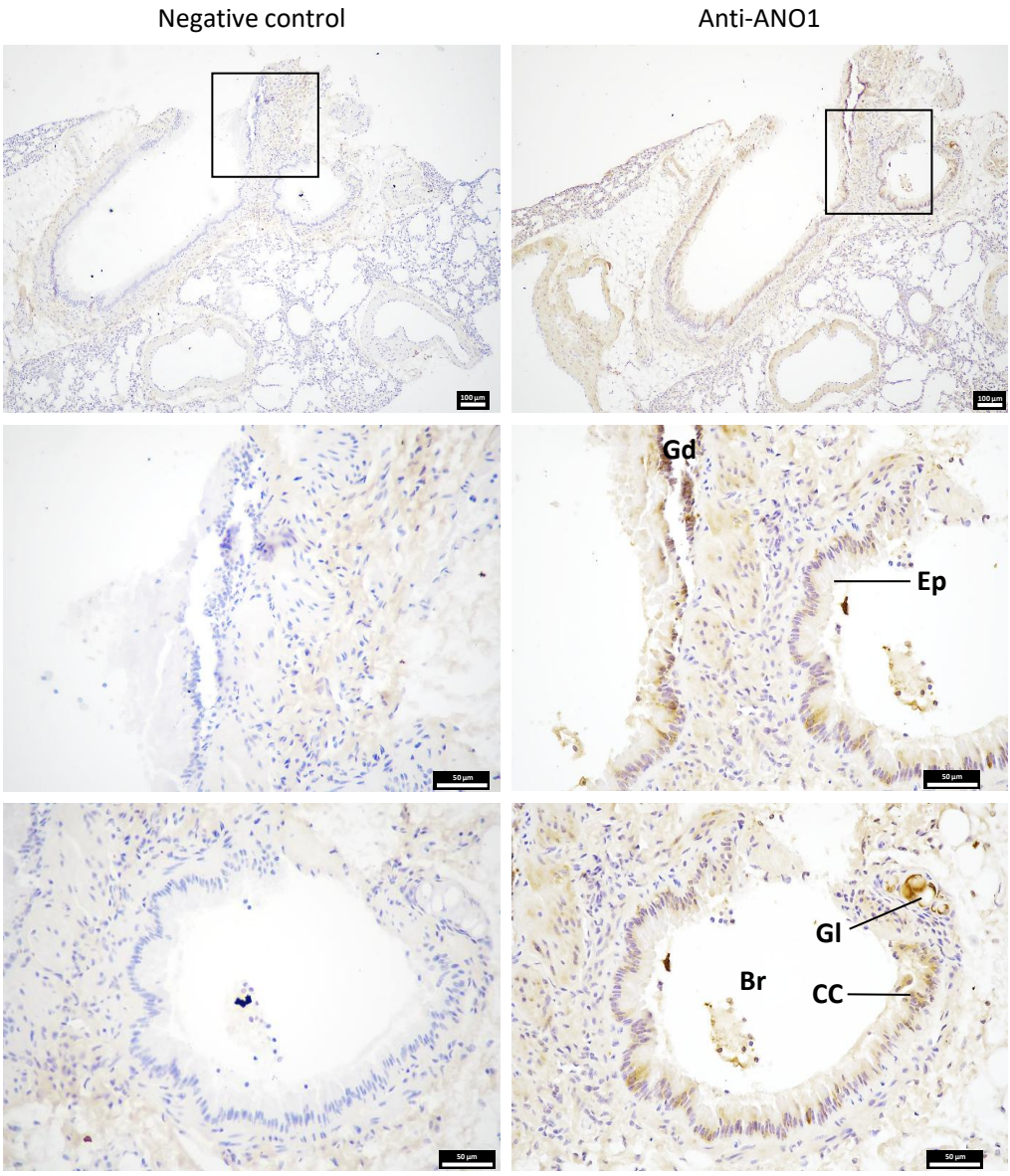


**Legend:** Immunohistochemical staining of lung tissue showing the expected ANO1 expression, confirming the specificity and functionality of the anti-ANO1 antibody (TMEM16A, ref. 12652-1-AP, Proteintech®), in WT mice aged 2–3 months (n = 3). Images shown at 10× and 40× magnification. Gl: gland; Br: bronchus; Ep: epithelium; CC: club cell; Gd: glandular duct.